

# Implications of surface flooding on airborne ~~estimatesthickness~~ measurements of snow depth on sea ice

Anja Rösel<sup>1,6\*</sup>, Sinead Louise Farrell<sup>2</sup>, Vishnu Nandan<sup>3</sup>, Jaqueline Richter-Menge<sup>4</sup>, Gunnar Spreen<sup>5,1</sup>, Dmitry V. Divine<sup>1</sup>, Adam Steer<sup>1</sup>, Jean-Charles Gallet<sup>1</sup>, and Sebastian Gerland<sup>1</sup>

<sup>1</sup>Norwegian Polar Institute, Fram Centre, Tromsø, Norway

<sup>2</sup>Department of Geographical Sciences, University of Maryland, College Park, MD, USA

<sup>3</sup>Centre for Earth Observation Science (CEOS), University of Manitoba, MB, Canada

<sup>4</sup>University of Alaska Fairbanks, Fairbanks, AK, USA

<sup>5</sup>Institute of Environmental Physics, University of Bremen, Bremen, Germany

<sup>6</sup>now at Remote Sensing Technology Institute, German Aerospace Center (DLR), Wessling, Germany

\*Correspondence to: Anja Rösel ([anja.roesel@dlr.de](mailto:anja.roesel@dlr.de))

**Abstract.** Snow ~~depththickness~~ observations from airborne snow radars, such as the NASA's Operation IceBridge (OIB) mission, have recently been used in altimeter-derived sea ice thickness estimates, as well as for model parameterization. A number of validation studies comparing airborne and in situ snow ~~depththickness~~ measurements have been conducted in the western Arctic Ocean, demonstrating the utility of the airborne data. However, there have been no validation studies in the Atlantic sector of the Arctic. Recent observations in this region suggest a significant and predominant shift towards a *snow-ice* regime, caused by deep snow on thin sea ice. During the Norwegian young sea ICE expedition (N-ICE2015) in the area north of Svalbard, a validation study was conducted on March 19, 2015. This study collected g-, during which ground truth data were collected during an OIB overflight. Snow and ice thickness measurements were obtained across a two dimensional (2-D) 400 m × 60 m grid. Additional snow and ice thickness measurements collected in situ from adjacent ice floes helped to place the measurements obtained at the gridded survey field site into a more regional context. Widespread negative freeboards and flooding of the ~~snowpacksnow-pack~~ were observed during the N-ICE2015 expedition, due to the general situation of thick snow on relatively thin sea ice. These conditions caused brine wicking into and saturation ~~of into~~ the basal snow layers. This causes, causing the airborne radar signal to undergo more diffuse scattering, resulting in the location of the radar main scattering horizon to be detected well above the snow/ice interface. This leads to a subsequent underestimation of snow depth, if only radar-based information is used. and influenced the airborne radar signal to detect the radar main scattering horizon well above the snow/sea ice interface, resulting in a subsequent underestimation of total snow depththickness, if only radar based information is used. The average airborne snow ~~depththickness~~ was 0.16 m thinner than that measured in situ at the 2-D survey field. Regional data within 10 km of the 2-D survey field suggested however a smaller

deviation between average airborne and in situ snow ~~depth~~thickness, a 0.06 m underestimate in snow ~~depth~~thickness by the airborne radar, which is close to the resolution limit of the OIB snow radar system. Our results also show a broad snow ~~depth~~thickness distribution, indicating a large spatial variability in snow across the region. Differences between the airborne snow radar and in situ measurements fell within the standard deviation of the in situ data (0.15 – 0.18 m). Our results suggest ~~that frequent~~that, with frequent sea water flooding of the snow/ice-ice interface ~~leads to underestimations in snow depth or overestimations of sea ice freeboard, measured from radar altimetry, in turn impacting the accuracy of sea ice thickness estimates. in specific regions of the Arctic in the future, may lead to an~~it may result in an underestimate of snow ~~depth~~thickness or an overestimate of ice freeboard, measured from radar altimetry, thereby affecting the accuracy of sea ice thickness estimates.

## 1 Introduction

Snow and sea ice thickness in a changing Arctic climate system are the matter of many recent studies (e.g. Webster et al. 2018), since the snow layer on top of the frozen ocean generates several contradictory effects on the polar climate. On the one hand, in winter, snow acts as an insulator between the relatively warm ocean and the cold atmosphere and hinders the heat exchange between ocean and atmosphere, reducing the sea ice growth rate (Sturm, 2002; Perovich, 2003). On the other hand, in spring and summer, ~~snow reflects~~ with its high optical albedo in the range of 0.7-0.85; ~~short-wave radiation and prevents the underlying sea ice with an albedo of about 0.6 from melting compared to about 0.6 for bare sea ice.~~ (Grenfell and Maykut, 1977, Perovich, 1996); ~~snow reflects short wave radiation and prevents the underlying ice from melting.~~ In addition, snow ~~cover controls the amount of transmittance of photosynthetically active radiation affecting the productivity of primary algae and phytoplanktons (Mundy et al., 2007). Moreover, snow~~ can be a positive contributor to the sea ice mass balance since snow can transform to snow-ice (Granskog et al., 2017; Merkouriadi et al., 2017a) and superimposed ice (Eicken et al., 2004; Wang et al., 2015).

Besides the importance of snow from a radiative and mass balance perspective, knowledge of snow ~~depth~~thickness on sea ice is also required for the accurate retrieval of sea ice thickness from satellite altimetry. The method relies on the assumption that sea ice floating in the ocean is in hydrostatic equilibrium, and sea ice thickness can be calculated by using observations of either ice-freeboard (from radar altimeters) or snow-freeboard (from laser altimeters) and assumptions about the respective densities of snow, ice and water. Ice- and snow-freeboard describe the distances above the local sea level to the snow/sea-ice or air/snow interface, respectively. The error budget of the derived ice thickness from laser altimetry is dominated by uncertainties of snow ~~depth~~thickness and ice and snow densities, ~~and~~ as well as uncertainties due to remaining errors in the sea surface height (Giles et al., 2007; Kern et al., 2015; Skourup et al., 2017).

Thus, accurate knowledge of snow ~~depth~~thickness on sea ice would be helpful to reduce the error in the sea ice thickness calculations and is important for quantifying climatological processes in Polar Regions. The Operation IceBridge (OIB) airborne campaigns (Koenig et al., 2010), which began in 2009, measure snow ~~depth~~thickness and surface elevation with an

ultra-wideband snow radar (e.g., Yan et al., 2017) and an airborne topographic mapper (ATM) laser altimetry system (Krabill et al., 2002), respectively. With ~~these~~~~this constellation of~~ sensors, both the air/snow and the snow/~~sea~~-ice interface can be detected with the snow radar (e.g., Newman et al., 2014), and the surface elevation can be mapped with the ATM (e.g., Farrell et al., 2012). Hence, the OIB data are a valuable source for validating satellite remote sensing sea ice products as well as for model parameterization. Furthermore, the comparison of airborne OIB data with in situ field measurements is necessary to understand the processes affecting radar penetration into snow covered sea ice and the impact of the snow load on the snow/~~sea~~-ice interface.

Several OIB validation studies have been conducted (e.g., Farrell et al., 2012; Webster et al., 2014; Newman et al., 2014; Holt et al., 2015), multiple snow ~~depth~~~~thickness~~ retrieval algorithms were developed (e.g., Kurtz et al., 2013, 2014; Newman et al., 2014; Kwok and Maksym, 2014), and ~~inter~~-compared with satellite products (Kwok et al., 2017; Lawrence et al., 2018). These studies have provided insights about the snow ~~depth~~~~thickness~~ uncertainty and the errors associated with the airborne techniques (Kwok, 2014; King et al., 2015). However, in the northern hemisphere, all evaluation studies (except those connecting to satellite data) have thus far focused on snow in the Canada Basin, in the central Arctic Ocean, or only in peripheral sub regions of the Arctic. To our knowledge, no OIB validation study has been conducted in the Atlantic sector of the Arctic.

-In recent years, a significant change towards thinner ice with thicker snow cover (Renner et al., 2014; Rösel et al., 2018) has been observed in this region, caused by an increase in intense storm events and associated precipitation in this area (Woods and Caballero, 2016; Graham et al., 2017; Rinke et al., 2017). In addition, previous studies indicate that radar signal penetration through the snow pack might be lower under certain geophysical snow-ice conditions in this area (Gerland et al., 2013; King et al., 2018; Nandan et al., 2020) and also in ~~the Weddell Sea ice in~~ the Antarctic (Kwok and Kacimi, 2018; ~~Willatt et al., 2009~~). Snow and ice conditions in this region differ to those in the Canada Basin and central Arctic (e.g., Webster et al., 2014; 2018), and they have been found to induce substantial negative ~~ice~~ freeboards with subsequent flooding of the snow pack, more akin to the conditions in the seasonal ice pack of the Southern Ocean (Massom et al., 2001). This may have an impact on remote sensing methods of snow and ice thickness estimation, which have so far only been validated for more typical Arctic conditions.

In this paper, we present in situ observations of sea ice and snow ~~depth~~~~thickness~~, and snow and ice characteristics from the N-ICE2015 expedition, alongside near-coincident airborne measurements acquired on 19 March 2015 during an OIB overflight. We calculate ice freeboard values from a variety of sensors to investigate the prevalence of negative freeboards and flooding at the snow/~~sea~~-ice interface. We investigate the impact of flooded snow layers on the airborne radar observations. Utilizing a combination of methodologies, we assess sea ice thickness conditions in the region. We discuss our results in the context of satellite-derived ice thickness and consider the impact of flooding on estimating thickness in regions with thin sea ice and deep snow, such as in the ~~Atlantic section of the Arctic Ocean or in the~~ Southern Ocean ~~or in the Atlantic sector of the Arctic Ocean~~.

## 96 2 Data and Methods

### 97 2.1 Study Area

98 Field observations for this study were acquired during the Norwegian young sea ICE expedition (N-ICE2015) with the  
99 research vessel *RV Lance*. The expedition started in the Arctic Ocean north of Svalbard at 83°15'N, 21°32'E on 15 January  
100 2015 and concluded at 80°N and 5°36'E on 22 June 2015 and consisted of a series of four drift segments (Granskog et al.,  
101 2016, 2018). In this study, we focus on sea ice and snow related observations from the drift of *Floe 2*, covering a time period  
102 from 24 February to 19 March 2015. Data from the OIB overflight employed in this study was collected on 19 March 2015  
103 at 82°29'N and 22°37'E above the drifting sea ice floe.

104  
105 The ice station on Floe 2 was set up on an aggregation of different ice types: refrozen leads, first year ice (FYI), and second  
106 year ice (SYI). Modal sea ice thickness at the field station was 0.3 m, 0.9 m, and 1.7 m, for refrozen leads, FYI, and SYI,  
107 respectively (Rösel et al., 2017). Snow ~~depth~~thickness was on average  $0.56 \pm 0.17$  m on FYI and SYI (Rösel et al., 2017),  
108 while on refrozen leads it was approximately 0.02 m, likely redistributed from blowing snow. For this study, a 400 m  $\times$  60 m  
109 survey field was established. Red flag poles, with black snow-filled trash bags, marked the outline making it visible from air  
110 (see Figure 1). Shortly after OIB overflights, snow depth and sea ice thickness ~~observations~~ were collected. On  
111 this two dimensional (2-D) survey field ~~using~~ ~~using a~~ “snake line” sampling pattern with 5 m spacing between lines across  
112 the short axis of the field (see Figure 1).

### 114 2.2 Ground-based measurements

115  
116 ~~S~~now ~~depth~~thickness measurements ( $h_{SP}$ , ~~N=1121~~1046) were obtained with a GPS snow probe (SP) from Snow-Hydro  
117 (Fairbanks, AK, USA). The snow probe is a thin pole with a sliding disk, 0.2 m in diameter. The pole penetrates the snow pack  
118 to the snow/sea ice interface, while the disk rests on the snow surface. Inside the pole a magnetic device measures the distance  
119 between the disk and the lower tip of the pole providing the snow ~~depth~~thickness (Sturm and Holmgren, 1999; 2018). Each  
120 measurement is time-tagged and geolocated, and recorded on a data logger. The accuracy of the measurements over sea ice  
121 may vary between  $\pm 1$ -3 mm (Marshall et al., 2006; Sturm and Holmgren, 2018) and the footprint is the size of the disk (i.e.,  
122 0.2 m). Snow ~~depth~~thickness measurements were made approximately every 5 m following the snake line sampling pattern  
123 within the 2-D survey field (see Figure 1).

124  
125 Total snow and ice thickness measurements ( $h_t$ , ~~N=1046~~7005) were obtained using the EM31 electromagnetic device (Geonics  
126 Ltd., Mississauga, Ontario, Canada). A person dragging the EM31 instrument on a plastic sledge followed the snow probe

sampler. The EM31 measurements were sampled with a frequency of 2 Hz. The footprint size of the EM31 ranges from 3 m to 5 m (e.g., Haas et al., 1997), depending on the ice and snow ~~depth~~thickness. The accuracy of the EM31 measurements is approximately  $\pm 0.1$  m (Haas et al., 2009) for level ice ~~and decreasing over deformed ice (Haas et al., 2009), but higher for rough and deformed ice.~~

For comparison to the EM31 data and to collect direct measurements, we drilled 10 equispaced holes ~~around the 2-D field perimeter~~ with a 2" auger ~~to and~~ measured ice ~~thickness, and~~ snow ~~depth~~thickness, ~~and and~~ ice freeboard. ~~Ice thickness observations were made~~ with a thickness gauge from Kovacs Enterprises (Roseburg, OR, USA). The gauge is a specific tape measure with a foldable metal weight at the bottom that can be deployed through the drill-holes. The accuracy of the readings is estimated to be  $\pm 0.01$  m. In addition, ~~both~~, a snow pit was dug in the vicinity of the 2-D survey field (Merkouriadi et al., 2017c) ~~to assess snow structure~~, and an ice core was obtained to measure ice salinity, temperature, and density (Gerland et al., 2017). The core was extracted with a 0.09 m diameter ice corer from Kovacs Enterprises (Roseburg, OR, USA).

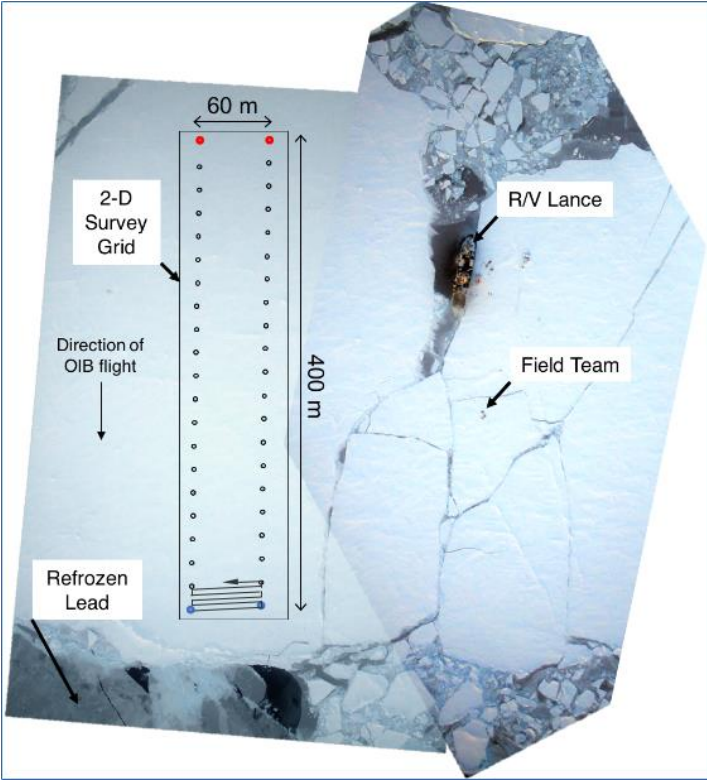
~~To provide a regional context for the observations made in the 2-D field, we use a set of long, and independent, transects with combined EM31 and snow depth~~thickness measurements (N=505360) obtained within a maximum radius of 5 km around the ~~ship d~~During the N-ICE2015 expedition, ~~a set of long, and independent, transects with combined EM31 and snow depth~~thickness measurements (N=5053) ~~were obtained within a maximum radius of 5 km around the ship.~~ These were performed to characterize the spatial variability of snow and ice thickness in the area surrounding the main ice camp. Further details can be found in Rösel et al. (2018). We use the ~~2-D grid snow depth measurements and those sampled via transects within a 5 km radius, to provide spatial representativeness and context from local- to regional-scales. results of the independent snow transects from Floe 2 and to provide the regional context for the measurements obtained in the smaller 2-D survey field.~~

### 2.3 Airborne measurements

The OIB aircraft surveyed the 2-D survey field three times (see Figure 2) on 19 March 2015. First a surveillance overflight occurred at 15:28 UTC. A second and third pass directly over the 2-D survey field occurred at 15:37 UTC and 15:43 UTC, respectively. Because the first pass did not adequately intersect the 2-D survey field, we focus our analysis on measurements obtained during passes 2 and 3 of the aircraft. Although the ice floe drifted during the airborne survey, the alignment of transects 2 and 3 were such that they directly intersected the 2-D survey field on both passes.

For sea ice studies, the aircraft was equipped with an ATM laser altimeter system (Krabill et al., 2002), an ultra-wideband frequency modulated continuous waveform (FMCW) snow radar system (e.g., Yan et al., 2017) and a digital camera system

160 (DMS) that provides high-resolution (0.1 m) geolocated visible-band images of the snow surface (Dominguez, 2018) allowing  
161 for visual interpretation of sea ice conditions in the vicinity of the 2-D survey field (see Figure 1).



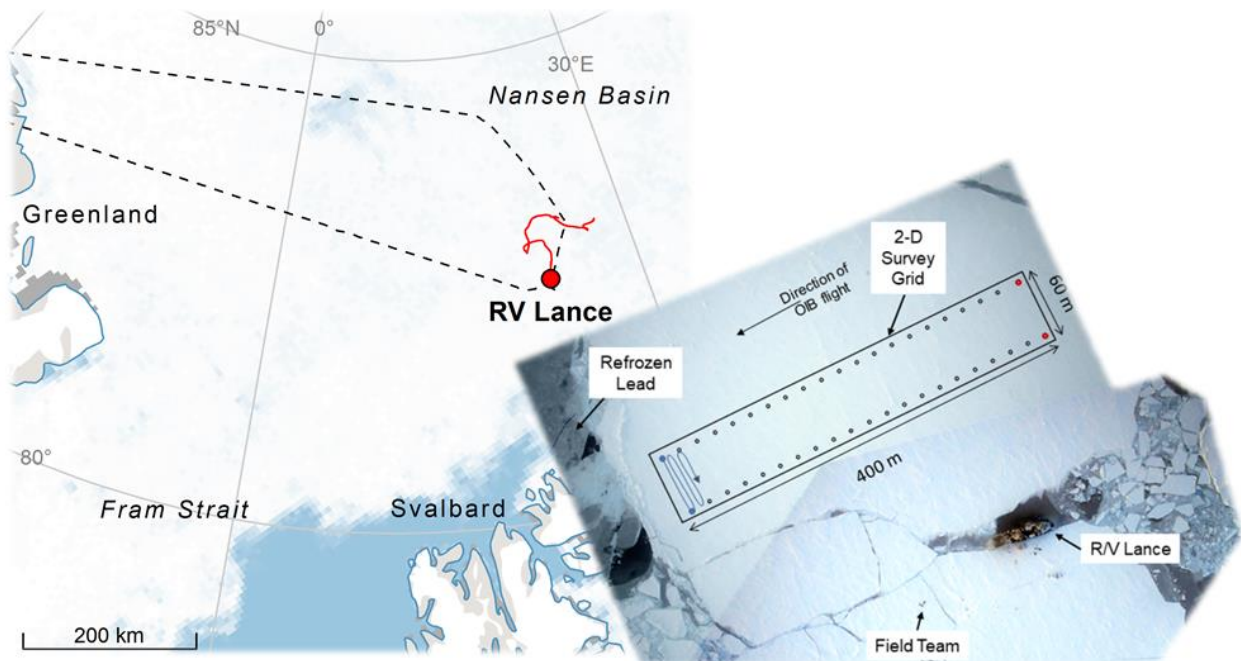


**Figure 1.** Overview of ~~survey-the~~ location in the Arctic Ocean (left) and setup of the 2-D in situ survey field situated on an ice floe as a part of the *floe 2* drifting phase to the west of *R/V Lance* on March 19, 2015 (right). Digital Mapping System (DMS) imagery (Dominguez, 2010, updated 2018) acquired during the OIB overflights were mosaicked to produce the aerials overview map. Black dots indicate the outline of the 2-D survey field. Snow and ice thickness measurements were obtained along the snake-line sampling pattern, as indicated in the lower-left of the figure survey field.



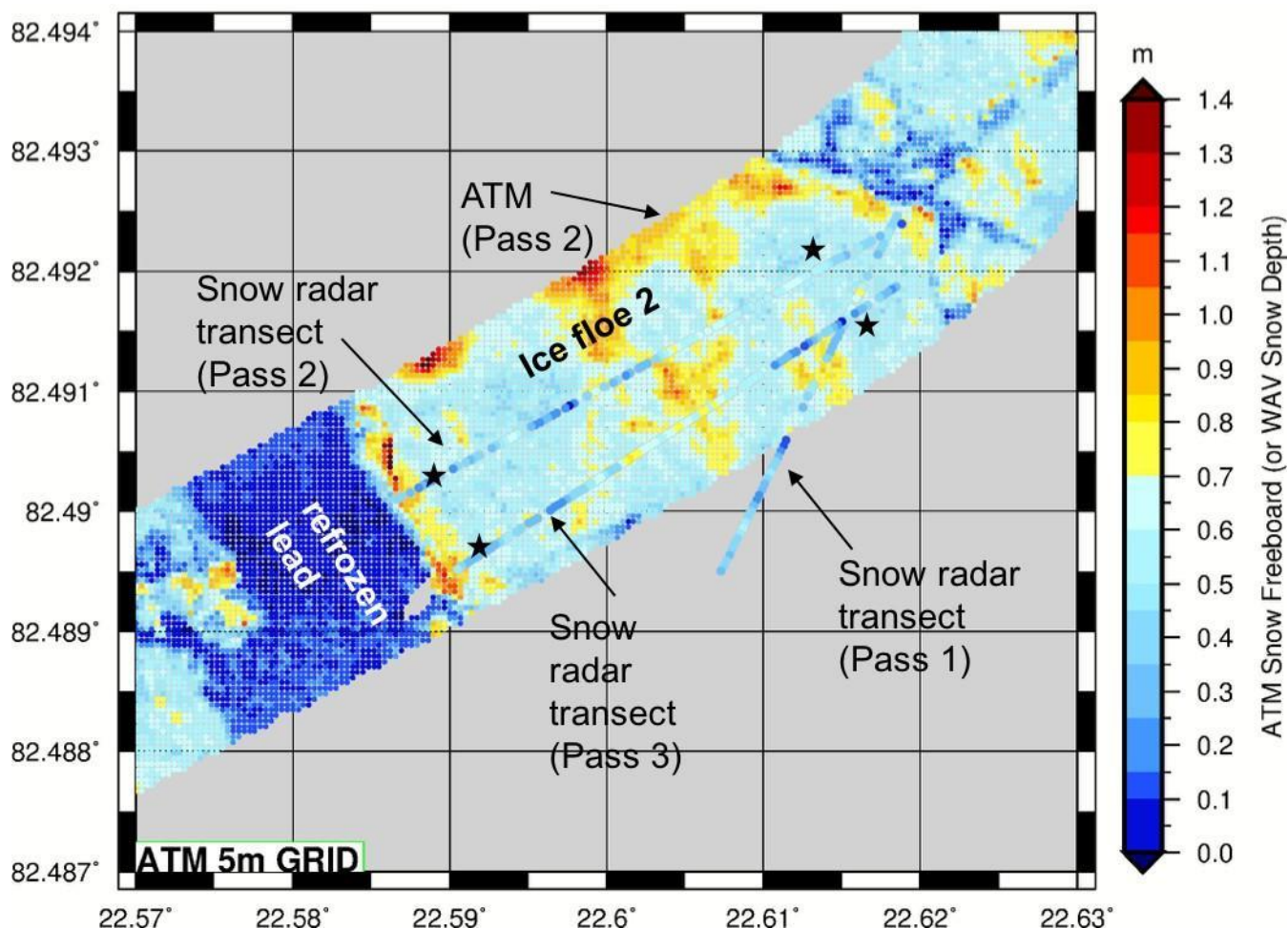


**Figure 2.** Detailed airborne mapping of the snow freeboard (5 m grid, derived from ATM observations of surface elevation) and snow depth (superimposed dots, derived from the airborne snow radar) at the 2-D survey field (corner points indicated by black stars) located on *Floe 2*. The three airborne transects across the field are indicated. During the OIB survey, the ice floe drifted south at an approximate drift speed of  $0.15 \text{ ms}^{-1}$ . [WAV Snow depth in the secondary y-axis refers to the snow depth retrieved using the NOAA Wavelet technique \(Newman et al., 2014\).](#)



187 **2.4 Methodology**

188 ~~We number the variables measured with the different observation techniques as follows: 1) derived from in-situ measurements~~  
189 ~~with EM31 and SP; 2) derived from in-situ measurements from drill holes; 3) derived from OIB measurements (ATM and~~  
190 ~~snow radar); 4) derived from a combination of in-situ and OIB measurements.~~

191 Table 1 summarizes all the variables used in the following context.

<u>suggested name</u>	<u>what it means</u>
<u>ht</u>	<u>combined snow depth + sea ice thickness</u>
<u>ht<sub>EM</sub></u>	<u>combined snow depth + sea ice thickness measured by EM</u>
<b><u>Total (snow + ice) freeboard / snow freeboard</u></b>	
<u>hfbs</u>	<u>Total freeboard generally</u>
<u>hfbs<sub>IS</sub></u>	<u>...from drill-holes</u>
<u>hfbs<sub>ATM</sub></u>	<u>...from laser scanner (ATM)</u>
<b><u>Sea ice thickness (the total ice component)</u></b>	
<u>hi</u>	<u>Sea ice thickness generally</u>
<u>hi<sub>IS</sub></u>	<u>...from drill-holes</u>
<u>hi<sub>EM,SP</sub></u>	<u>...estimated from EM and snow probe</u>
<u>hi<sub>ATM,SP</sub></u>	<u>from ATM total freeboard, snow probe depths and densities</u>
<b><u>Snow depth</u></b>	
<u>hs</u>	<u>Snow depth generally</u>
<u>hs<sub>IS</sub></u>	<u>...from drill-holes or snow pits</u>
<u>hs<sub>SP</sub></u>	<u>...from snow probes</u>
<u>hs<sub>SR</sub></u>	<u>...from radar</u>

<u>Ice freeboard (no snow)</u>	
<u>hfb</u>	<u>Ice freeboard generally</u>
<u>hfb<sub>IS</sub></u>	<u>...from drill-holes</u>
<u>hfb<sub>ATM,SR</sub></u>	<u>...from ATM and snow radar</u>
<u>hfb<sub>EM,SP</sub></u>	<u>...estimated from EM and snow probes</u>
<u>hfb<sub>ATM,SP</sub></u>	<u>...estimated from lidar and snow probes</u>

Table 1: Overview of variables used in this study

#### 2.4.1 Drift correction

~~To In order to~~ obtain spatial coincidence between the in situ and airborne measurements of snow ~~depth~~thickness, freeboard and sea ice thickness, ~~and~~ the positions of all measurements were ~~first~~ corrected to mitigate the impact of the drifting sea ice during the experiment. As a reference, we determined the position of the four corners of the 2-D survey field using the DMS imagery collected during the second and third OIB overpasses. ~~We extracted the precise latitude and longitude from the geo-referenced DMS imagery and by~~ comparing the differences for each corner marker between the two overpasses, we were able to deduce that the ice floe was drifting south at a speed of  $0.15 \text{ ms}^{-1}$ . To correct for the drift that occurred during the EM31 and SP sampling of the 2-D survey field, we followed the procedure described in Rösel et al. (2018): The EM31 data was resampled onto the coordinates of the SP track, and a Gaussian filter was applied to the EM31 data. Afterwards, both the EM31 and the SP data were interpolated~~median sampled~~ on a 5 m regular grid. ~~to avoid oversampling (Geiger et al., 2015).~~

#### 2.4.2 Density of sea water, ice and snow

In all calculations we used the following values: the density for sea water was  $\rho_W = 1027 \text{ kgm}^{-3}$  (Meyer et al., 2017), the bulk density for the snow pack was  $\rho_s = 328 \text{ kgm}^{-3}$  (Merkouriadi et al., 2017b), and the bulk density for FYI was  $\rho_i = 910 \text{ kgm}^{-3}$  (Gerland et al., 2017). All values are based on ~~actual~~ measurements obtained during the N-ICE2015 expedition at floe 2.

#### 2.4.3 In situ snow ~~depth~~thickness, sea ice thickness, and freeboards

In Figure 3, the concept of isostatic equilibrium is shown for four cases: On the left side, the ratio of snow ~~depth~~thickness ( $h_s$ ) to sea ice thickness ( $h_i$ ) is smaller, resulting in a positive sea ice freeboard ( $hfb$ ) or ice freeboard at sea level. On the right side, the situation of the 'new' Arctic as described in Rösel et al. (2018) is schematically presented: A thick snow layer  $h_s$  is

pushing a relatively thin sea ice  $h_i$  layer below the ocean surface. The resulting sea ice freeboard  $hfb$  becomes negative, and subsequently the sea ice surface is vulnerable ~~to~~<sup>for</sup> flooding.

To obtain sea ice thickness ( $hi_{EM,SP}$ ) from SP and EM31~~the in-situ~~ measurements, the resampled snow depth measurements from SP ( $hs_{SP}$ , N=1046) were subtracted from the total sea ice thickness from EM31 measurements ( $ht_{EM}$ , N=1046):

$$hi_{IS} = ht_{EM} - hs_{SP} \quad (1)$$

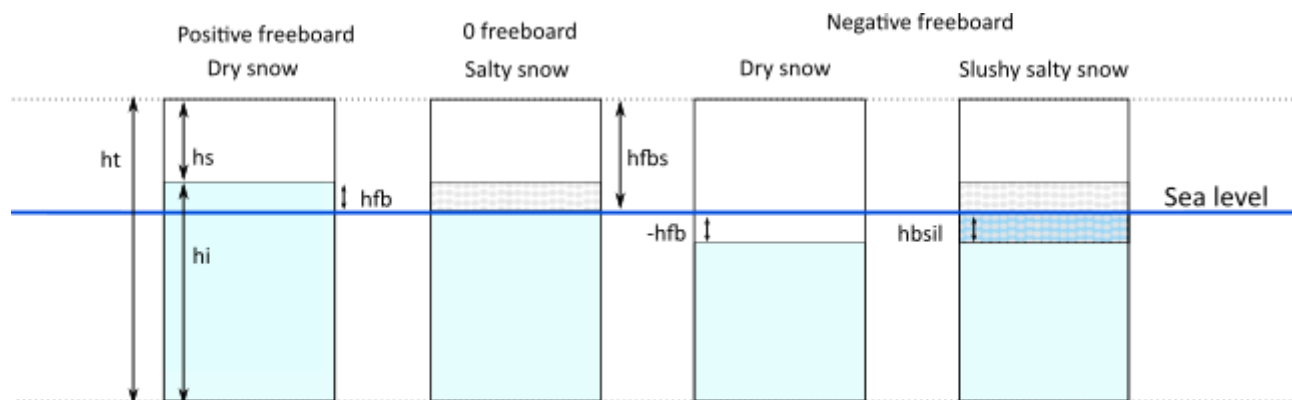
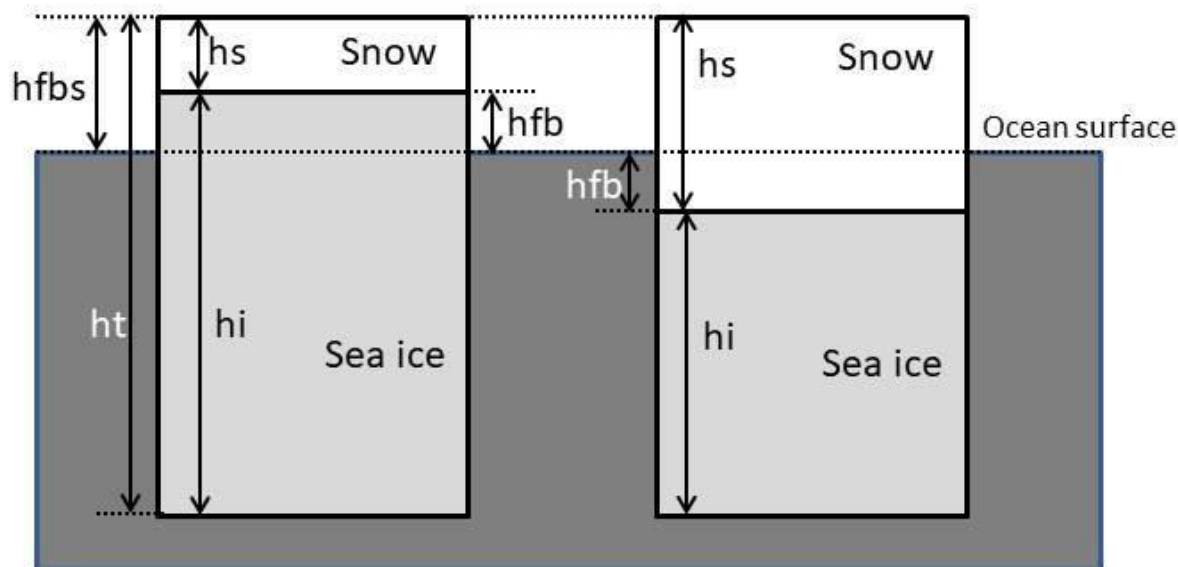


**Figure 3:** Some examples to show the concept of isostatic equilibrium of sea ice: On the left (a), the ratio of snow depth/thickness ( $h_s$ ) to sea ice thickness ( $h_i$ ) is small, sea ice freeboard ( $hfb$ ) is positive. On the right (c, d), the ratio of  $h_s$  to  $h_i$  is high,  $hfb$  is negative. In the second example (b), while the sea ice freeboard ( $hfb$ ) is zero, the lower part of the snow pack can be salty from wicked-brine wicking. This can also occur for positive ice freeboards. Example d) shows a slushy salty

snow layer ( $hfb_{sil}$ ) due to surface flooding, whereas example c) has a dry, non-salty snow cover. The snow freeboard  $hfb_s$  is the same in ~~all four~~<sup>both</sup> cases.

Assuming isostatic equilibrium assumption,  $hi_{EM,SP}$  under dry snow conditions can ~~be~~ calculated as:

$$hi_{EM,SP} = hfb_{EM,SP} \left( \frac{\rho_W}{\rho_W - \rho_i} \right) - \left( \frac{\rho_W - \rho_s}{\rho_W - \rho_i} \right) h_{SP} \quad (2)$$

which results in the freeboard ( $hfb_{IS}$ ) derived from the in situ ( $IS$ ) measurements using obtained snow ~~depth~~<sup>thickness</sup> and sea ice thickness information and densities given above:

$$hfb_{EM,SP} = \frac{hi_{EM,SP}(\rho_W - \rho_i) + (\rho_W - \rho_s)h_{SP}}{\rho_W} \quad (3)$$

For wet snow conditions, or a flooded state of the sea ice, we refer to the studies of Zwally et al., 2008 and Ozsoy-Cicek et al., 2013, where either  $h_s$  is set equal to  $hfb_s$ , or a slush layer is included in the calculations, respectively. In addition, we gain in situ information from the drill-hole readings: Sea ice thickness ( $hi_{IS}$ ), snow ~~depth~~<sup>thickness</sup> ( $hs_{IS}$ ), freeboard ( $hfb_{IS}$ ), and snow freeboard ( $hsfb_{IS}$ )

$$hsfb_{IS} = hfb_{IS} + hs_{IS} \quad (4)$$

As described in Rösel et al., 2018 the uncertainty ~~of in situ freeboards  $hfb_{EM,SP}$  and  $hsfb_{EM,SP}$  resulting from the propagation of uncertainties in the snow and ice densities and the sampling uncertainty. (represented by the spatial variability)~~ The measurement accuracy of in situ freeboards  ~~$hfb_{EM,SP}$  and  $hsfb_{EM,SP}$~~  is estimated to be ~~on average  $\pm 0.06$  m. to be on average  $\pm 0.06$  m. ; T~~ The accuracy of freeboard from the drill-hole measurements  $hfb_{IS}$  and  $hsfb_{IS}$  is  $\pm 0.01$  m (Rösel et al., 2018).

#### 2.4.4 Airborne snow ~~depth~~<sup>thickness</sup>, sea ice thickness, and freeboards

The DMS images were used to identify the geographical coordinates of areas of open water (with little or no ice cover) within the large refrozen lead, located in the southwest of the 2-D survey field site and adjacent to it (see Figure 1). ATM elevation measurements associated with these areas were averaged to estimate the local sea surface height (SSH). The SSH within the lead was then subtracted from all ATM elevations, to obtain the ATM snow freeboard ( $hsfb_{ATM}$ ). Individual ATM

measurements were resampled on the same 5-m regular grid as the in situ snow and ice measurements across the sea ice floe (see Figure 2). The snow radar echoes from passes 2 and 3 from the OIB survey also illustrate the presence of open water, refrozen leads and areas with deep snow cover on the N-ICE2015 ice floe (see Figure 4).

We calculated snow ~~depth~~~~thickness~~ from snow radar ( $h_{SR}$ ), following the methodology of Newman et al. (2014). Since the basal snow layers were saline in some locations, the snow/~~sea~~-ice interface could not always be detected. Therefore, a running average at 25 m length-scale (equivalent to five snow radar measurements) was used to account for an observed diffuse snow/~~-~~ice interface at the 2-D survey field site, possibly caused by a saline basal layer in the lower snow pack.

Ice freeboard ( $hfb_{ATM,SP}$ ) and sea ice thickness ( $hi_{ATM,SP}$ ) derived from a combination of the airborne data measurements acquired over the 2-D survey field site with the in situ snow-probe data were calculated as follows:

$$hfb_{ATM,SP} = h\del{sf}bs_{ATM} - h_{SR} \quad (5)$$

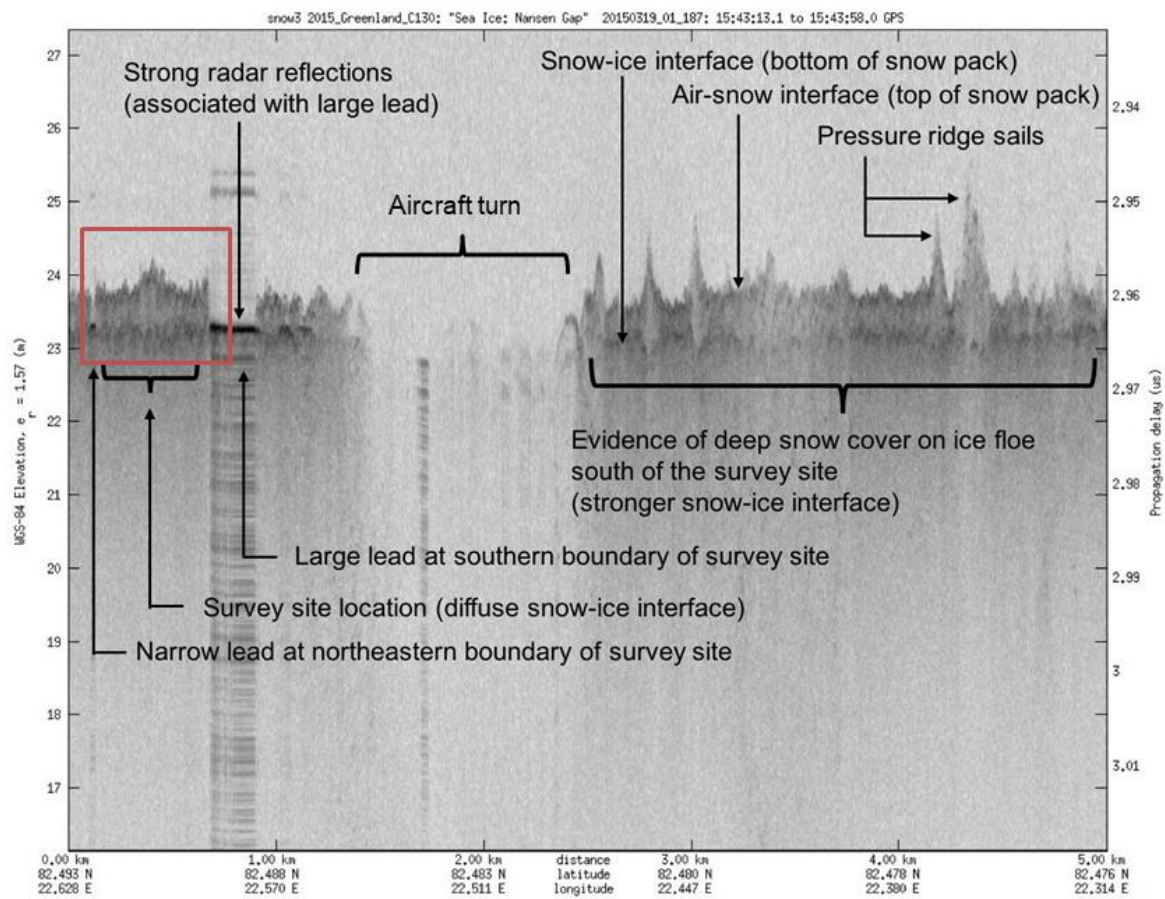
$$hi_{ATM,SP} = \frac{\rho_W hfb_{ATM,SP}}{\rho_W - \rho_i} + \frac{\rho_s h_{SR}}{\rho_W - \rho_i} \quad (6)$$

~~In addition, ice freeboard can be calculated through the~~ Here we introduce the term  $hB$  which is the difference between the ATM snow freeboard ( $h\del{sf}bs_{ATM}$ ) and the snow radar snow ~~depth~~~~thickness~~ ( $h_{SR}$ ).  ~~$hB - hfb_{ATM,SR}$  is effectively the freeboard of a radar reflecting layer, including used to indicate the depth of the ice freeboard plus a~~ ~~the~~ frozen snow-ice basal layer, if present.

$$\del{hB}hfb_{ATM,SR} = hfb + hbsil + E = h\del{sf}b\del{3}hfb_{ATM} - h_{SR} \quad (7)$$

Where  $hfb$  is the ice freeboard,  $hbsil$  is the thickness of the slushy snow-ice basal layer, and  $E$  is any remaining errors due to the interface picking algorithms as applied to the snow radar echos (Figure 4).





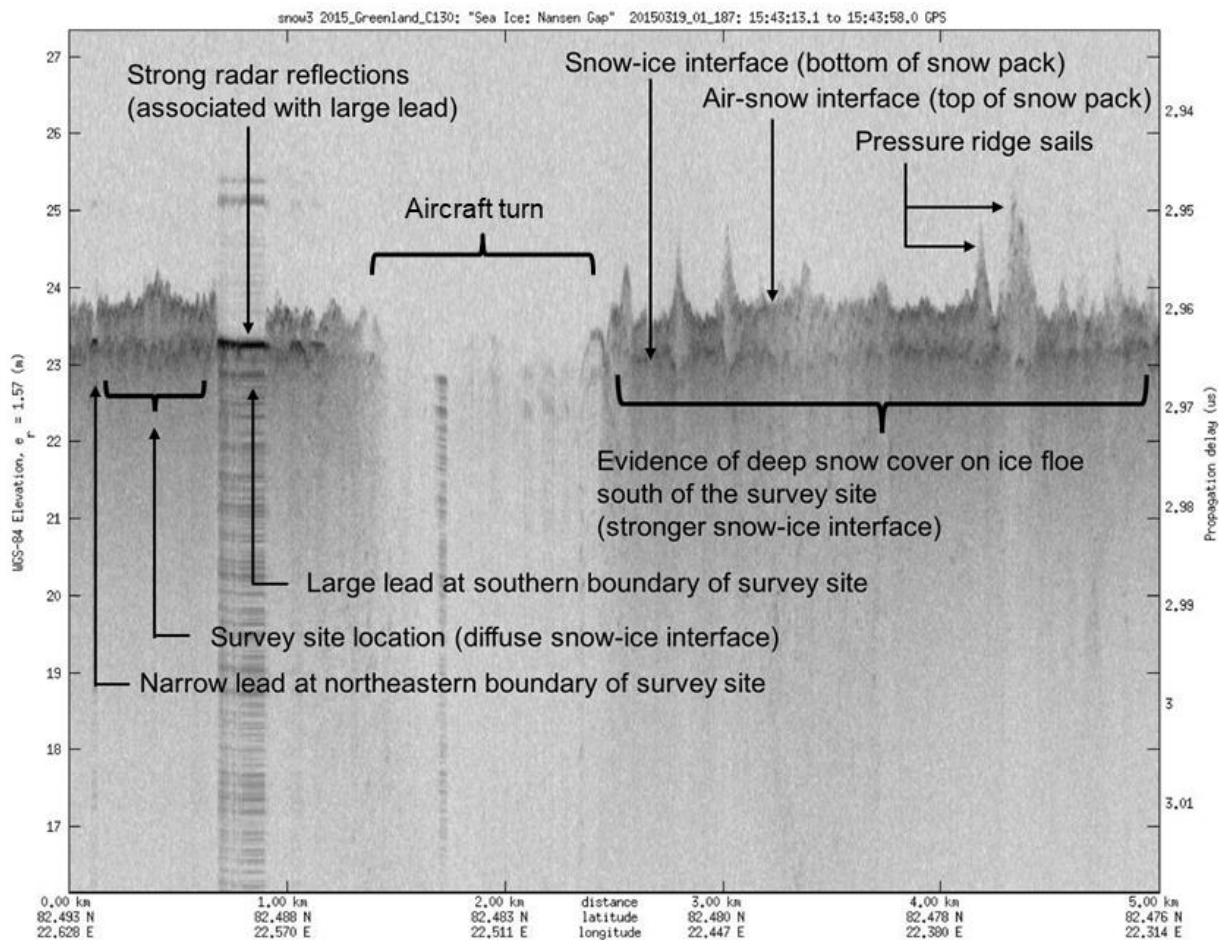


**Figure 4:** Processed and annotated OIB snow radar echo surveyed from the 2-D survey field, during the ~~second and~~ third pass on 19 March 2015 ~~at. The second and third passes were was acquired at 15:37 UTC and~~ 15:43 UTC. ~~The red bounding box indicates the close-ups of the regions as shown in Figures 1 and 2.~~

### 3 Results

#### 3.1 In situ and airborne measurements from the 2-D survey field site and their comparison

The salinity profile of ~~an~~the ice core, taken on 5 March 2015 ~~at~~in the vicinity of the 2-D survey field site, shows a typical C-shape profile with relatively high salinity values up to 11.3 psu at the top and 5.8 psu at the bottom, respectively, and lower

values of between 1.3 psu and 4.3 psu in the middle sections of the ice core (see Figure 10 in Appendix) suggesting that the 2-D survey field site on the ice floe comprised of FYI.

The average calculated sea-ice thicknesses ( $h_{IS}$ , eq. 1) on the 2-D survey field site is  $1.50 \pm 0.28$  m with a mode of 1.40 m, and the average snow depth thickness measured with the snow probe is  $h_{SP} = 0.58 \pm 0.15$  m with a mode of 0.55 m (results summarized in Table 42). The drill-hole measurements lie within the standard deviation of all measurements collected at the 2-D survey field site, i.e. our results demonstrate very good agreement across all observation methods (Figure 5 and Table 23 in Appendix). Three out of the ten drill-holes were found to be flooded.

For direct comparison of the in situ sampled snow depth and ice thickness data, a subset of the snow radar data of both overpasses over the 2-D survey field site, limited by the 4 corner coordinates of the 2-D survey field ( $N=22762$ ), results in an average snow depth thickness of  $h_{SR} = 0.42 \pm 0.16$  m, with a second mode of 0.40 m, 0.16 m and 0.15 m lower than the mean and modal snow depth thickness of 0.55 m measured in situ at the 2-D survey field site, respectively ( $N=1046$ , Figure 5a). However, the standard deviations, i.e. the width and shape of the snow depth thickness distributions, for both the in situ and airborne snow radar observations are in very good agreement with values of 0.15 m and 0.16 m, respectively. In addition, the average snow depth thickness from the airborne snow radar was 0.08 m larger than average snow depth at the drill-hole locations  $h_{IS} = 0.50 \pm 0.18$  m ( $N=10$ , Figure 5a).

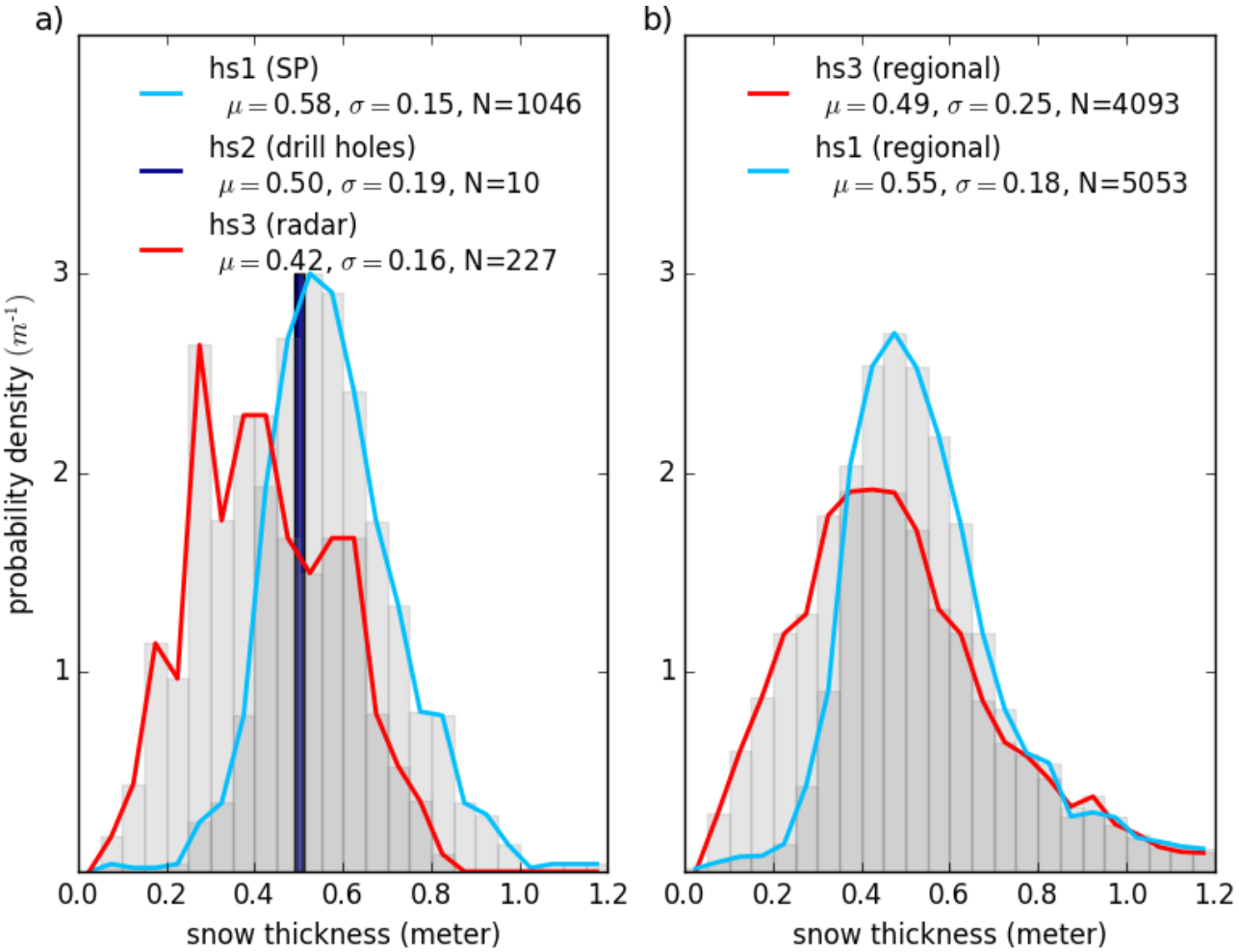
### 3.2 Local- vs regional-scale snow depth and sea ice thickness measurements

During the N-ICE2015 expedition, long transects on different predefined lines with combined EM31 and snow depth thickness measurements were performed to examine the spatial variability of the area surrounding the main ice camp and included measurements of thin ice and deformed ice areas (Rösel et al., 2018). Altogether, five transects with 5053-5060 gridded snow and ice measurements were made on Floe 2, covering a time period from 24 February to 19 March 2015, which resulted in an average snow depth thickness of  $0.55 \pm 0.18$  m and an average sea ice thickness of  $1.09 \pm 0.92$  m.

As shown in Rösel et al. (2017), the overall measurements on the local area scale are representative of sea ice in the region. To gain knowledge about the agreement in the snow depth thickness between the airborne and in situ observations on a more regional scale, we compared observations from snow radar within a 10 km radius around the position of R/V Lance with the average in situ snow depth thickness transect measurements conditions measured in situ during the drift of Floe 2 during the N-ICE2015 expedition within a 5 km radius of the ship. Similar to the results obtained at the 2-D survey field site, the snow distributions show an offset for the airborne snow radar data towards lower snow depth thickness values. The average snow depth thickness from the airborne snow radar was  $0.49 \pm 0.25$  m, 0.06 m below the average snow depth thickness of  $0.55 \pm 0.18$  m measured directly with the SP (Figure 5b). While the one-to-one comparison over the survey field can be considered as a direct validation study, the statistical regional comparison across the larger area can potentially be influenced by geophysical and thermodynamic processes such as ice dynamics, snow redistribution, snow metamorphism etc. that occurred during the entire drift duration of floe 2 (23 days) where in situ data were acquired.

324 The drill hole measurements made at the 2-D survey field site (N=10) gave the following averaged results: ice thickness  $hi2_{IS}$   
 325  $= 1.39 \pm 0.33$  m, snow depththickness  $hs2_{IS} = 0.50 \pm 0.18$  m, freeboard (FB2)  $hfb2_{IS} = 0.01 \pm 0.07$  m and snow freeboard  
 326  $hsfb2_{IS} = 0.50 \pm 0.12$  m (see Table 2 in Appendix). These values lie within the standard deviation of all measurements  
 327 collected at the 2-D survey field site, i.e. our results demonstrate very good agreement across all observation methods. Three  
 328 out of the ten drill holes were flooded, already before drilling.

329  
 330  
 331



332 **Figure 5.** Probability density functions of snow depththickness measurements with given average values ( $\mu$ ), standard  
 333 deviations ( $\sigma$ ), and number of measurements (N) from a) the in 2-D survey field site, obtained with the snow probe (blue)  
 334

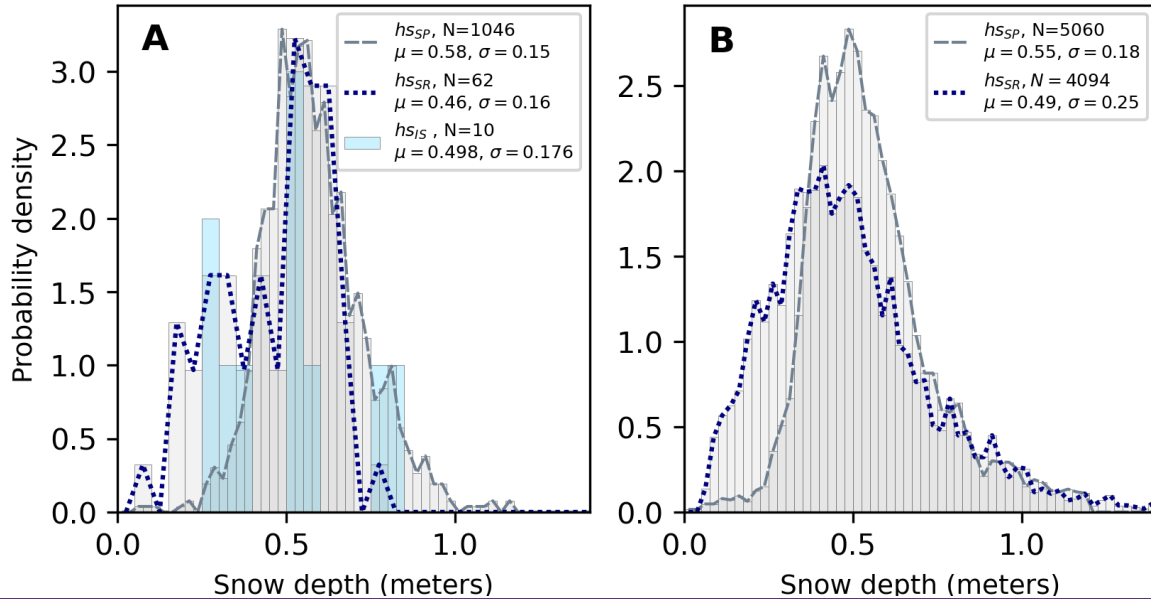


Figure 5. Probability density functions of snow depth measurements with given average values ( $\mu$ ), standard deviations ( $\sigma$ ), and number of measurements ( $N$ ) from a) the in 2-D survey field site obtained with the snow probe (grey dashes), the OIB snow radar (blue dots) and drill-holes (light blue bars); b) a wider surrounding from snow probe sampling during the entire N-ICE2015 - floe 2 campaign (grey dashes) and from OIB snow radar within a radius of 10 km around the position of R/V Lance (blue dots).

For comparison with the ice freeboard,  $hfb_{IS} = 0.01 \pm 0.07$  m, observed at the drill-hole sites, we used the ~~in-situ~~ in-situ ground measurements, i.e. SP and EM31, to derive freeboard ~~(FB)~~  $hfb_{EM,MPIs} = -0.02 \pm 0.05$  m with an uncertainty of  $\pm 0.06$  m (Rösel et al., 2018), following eqn. 3.

While the average freeboard at the 2-D survey field site is close to ~~0.00~~ 0.00 m based on the drill-hole measurements alone, the distribution of freeboards shown in Figure 6 ~~are negative, with magnitudes up to 0.1 m.~~ illustrates that a significant fraction of  $hfb_{IS}$ -values lie in the negative range, to -0.1 m. Results in the same range are obtained by subtracting the snow probe measurements from ATM surface elevation, resulting in, with an average value of  $hfb_{ATM,SP} = 0.03 \pm 0.09$  m, are obtained by subtracting the snow probe measurements from ATM surface elevation ( $hfb_{ATM,SP}$ ), see Figure 6). Taking the  $\pm 0.06$  m

uncertainty into account, this results in a negative freeboard area fraction of 19% and 14% across the 2-D survey field site for  $FB1-hfb_{EM,SP}$  and  $FB4hfb_{ATM,SP}$ , respectively (see Figure 7). An estimate of the ice freeboard plus the thickness of the snow-ice basal layer at the survey site that was impacted by brine wicking may be obtained by subtracting the snow radar measurements from the nearest ATM surface elevation value, which results in an average  $hBfb_{ATM,SR} = 0.20 \pm 0.10$  m but varies across the site (Figure 7c). The subsequent difference between  $hBfb_{ATM,SR}$  and  $hfb_{ATM,SP}$  provides an approximate estimate of the thickness of the flooded, slushy, snow-ice basal layer of the snow cover.

	snow <u>depth</u> <del>thickness</del> ( $h_{S_s}$ ) [m]	sea ice thickness ( $h_{i_i}$ ) [m]	snow freeboard ( $h_{sfb_s}$ ) [m]	sea ice freeboard ( $hfb$ ) [m]
(1) in situ (EM31/SP)	0.58±0.15	1.50±0.28	0.54±0.09	<u>0.03-0.02±0.095</u>
(2) in situ (drill-holes )	0.50±0.18	1.39±0.33	0.50±0.12	0.01±0.07
<u>OIB (Snow radar, inside 2D field)</u>	<u>0.46±0.16</u>			
(3) OIB (Snow Radar)	0.42±0.16			
(3) OIB (ATM)			0.62±0.10	
(4) OIB (ATM/in situ)		<u>1.90±0.62</u> (1.52±0.57)		0.03±0.09

**Table 12:** Results of snow, sea ice, and freeboard measurements and calculations of the 2-D survey field site

Finally, in Figure 8, we show the sea ice thickness distributions collected at the 2-D survey field site  $hi_{EM,SP}$   ~~$hi_{EM,SP1}$~~  and  $hi_{IS}$   ~~$hi_{IS2}$~~ , as well as for the region surrounding the *R/V Lance*,  $hi_{ATM,SR}$  (all)  ~~$hi_{REGIONAL}$~~ . For comparison we include  $hi_{ATM,SP}$   ~~$hi_{ATM,SP4}$~~ , calculated from a combination of the ATM data and the in situ snow probe measurements. The ~~in situ~~ in situ measurements show that the 2-D survey field site was situated on an ice floe ranging between 1.4 and 1.5 m thick ~~1.4 to 1.5 m thick~~ (Figure 8). This compares to a slightly-regional-scale thinner ~~overall~~ ice cover regionally ~~(1.09 ± 0.92m)~~, as measured from Floe 2. The variability in sea ice thickness in the region surrounding the *R/V Lance* is about three times larger than that at the 2-D survey field site. We note that the average sea ice thickness  $hi_{ATM,SP}$   ~~$hi_{ATM,SP}$~~  = 1.90 m is biased high because the thickness equation (eqn. 6) does not take into account the two-layer snow set-up, with each snow layer having a different depth and density. Our results suggest that the resulting ~~resulting~~ bias is approximately 0.4 m, and ~~and~~ this is consistent with the result shown in Figure 6, which indicates a bias of approximately 0.03 m in  $hfb_{EM,SP}$   ~~$FB1$~~ . This bias might be caused, which arose for by the same reason (i.e., eqn. 2 also does not account for the two-layer snow situation).



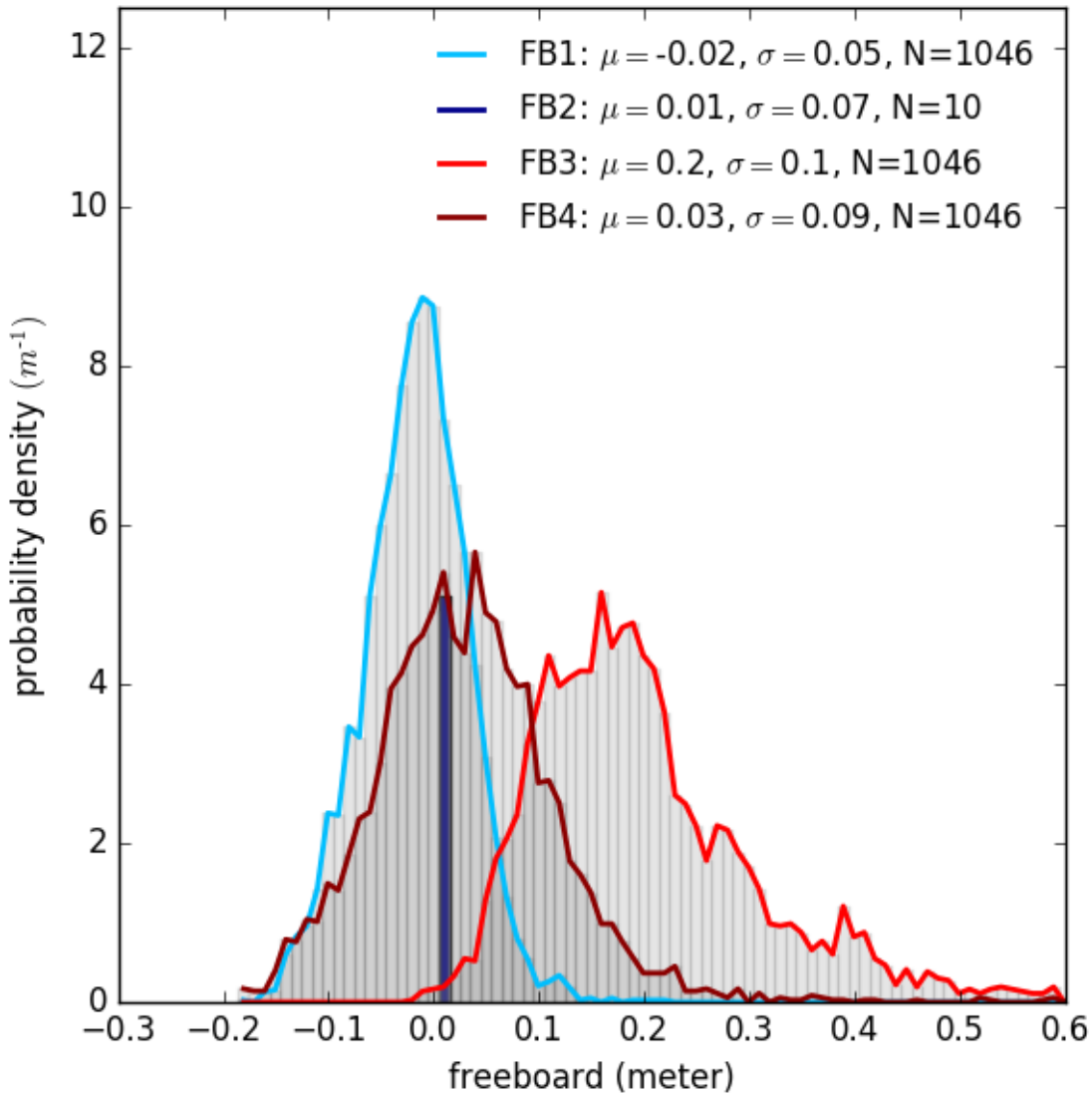


**Figure 6:** PDFs of freeboards (FB) with given average values ( $\mu$ ), standard deviations ( $\sigma$ ), and number of measurements ( $N$ ) from the 2-D survey field site. FB1 (light blue): Freeboard calculated from SP snow depth thickness, sea ice thickness from EM31 and densities of snow, ice and water, and assuming a hydrostatic equilibrium sea ice thickness; FB2 (dark blue): Freeboard from drill hole measurements; FB3 (red): Freeboard derived from ATM surface elevation minus average snow depth thickness of SR measurements; FB4 (dark red): Freeboard derived from ATM surface elevation minus snow depth thickness of SP measurements. Detailed descriptions of the methods are given in the text.

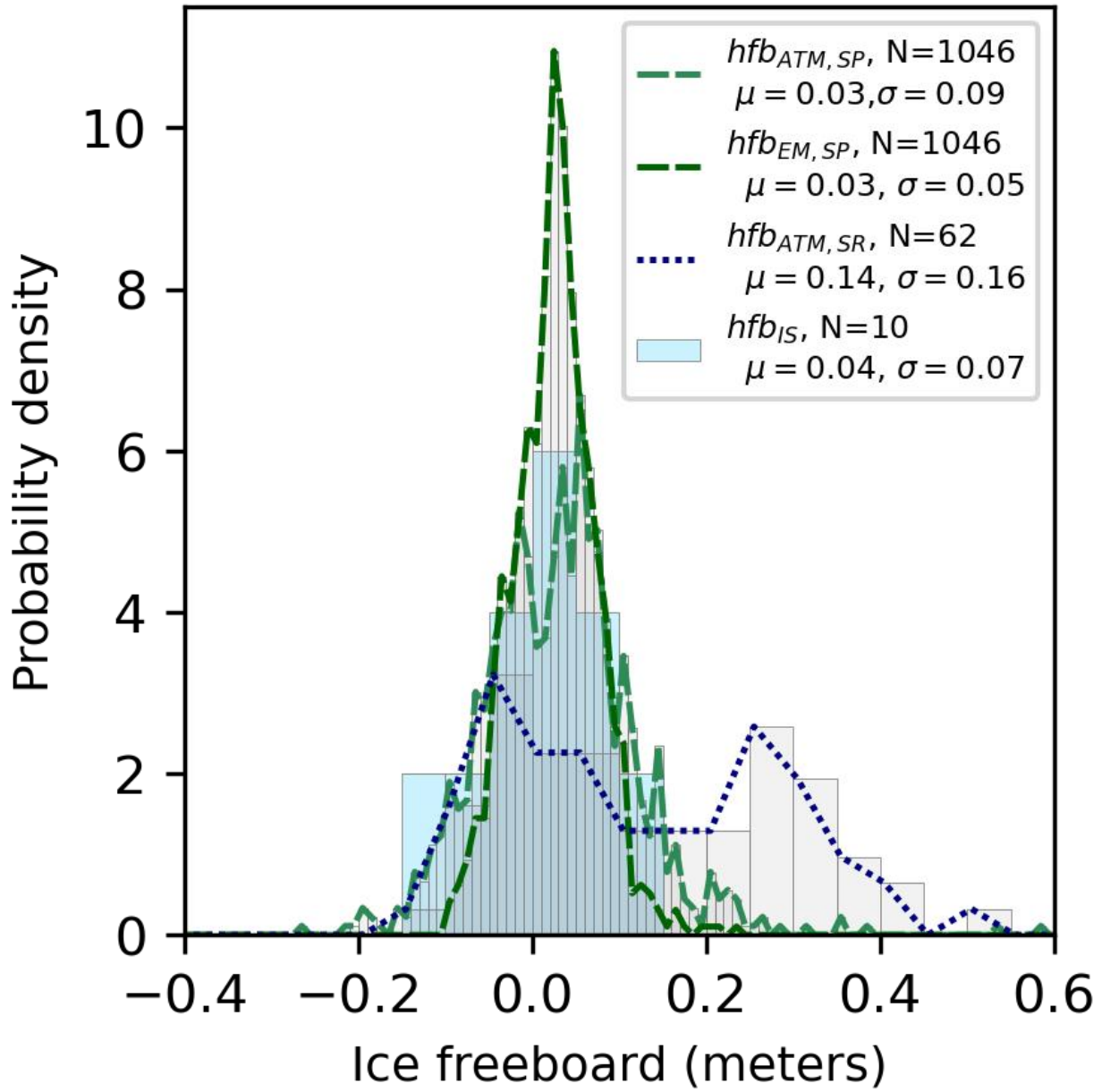


**Figure 6:** PDFs of ice freeboard ( $h_i$ ) with given average values ( $\mu$ ), standard deviations ( $\sigma$ ), and number of measurements ( $N$ ) from the 2-D survey field site.  $hfb_{ATM,SP}$  (light green dashes): freeboard calculated from SP snow depth and ATM surface elevations using Equation 2;  $hfb_{EM,SP}$  (dark green dashes): ice freeboard from EM and SP measurements;  $hfb_{ATM,SR}$  (dark blue

dots): ice freeboard derived from ATM surface elevation minus matched SR snow depths within the 2-D field;  $hfb_{IS}$  (light blue bars): ice freeboard from drill-hole observations on 2-D field edges, plotted as a regular histogram for tidy visualisation.

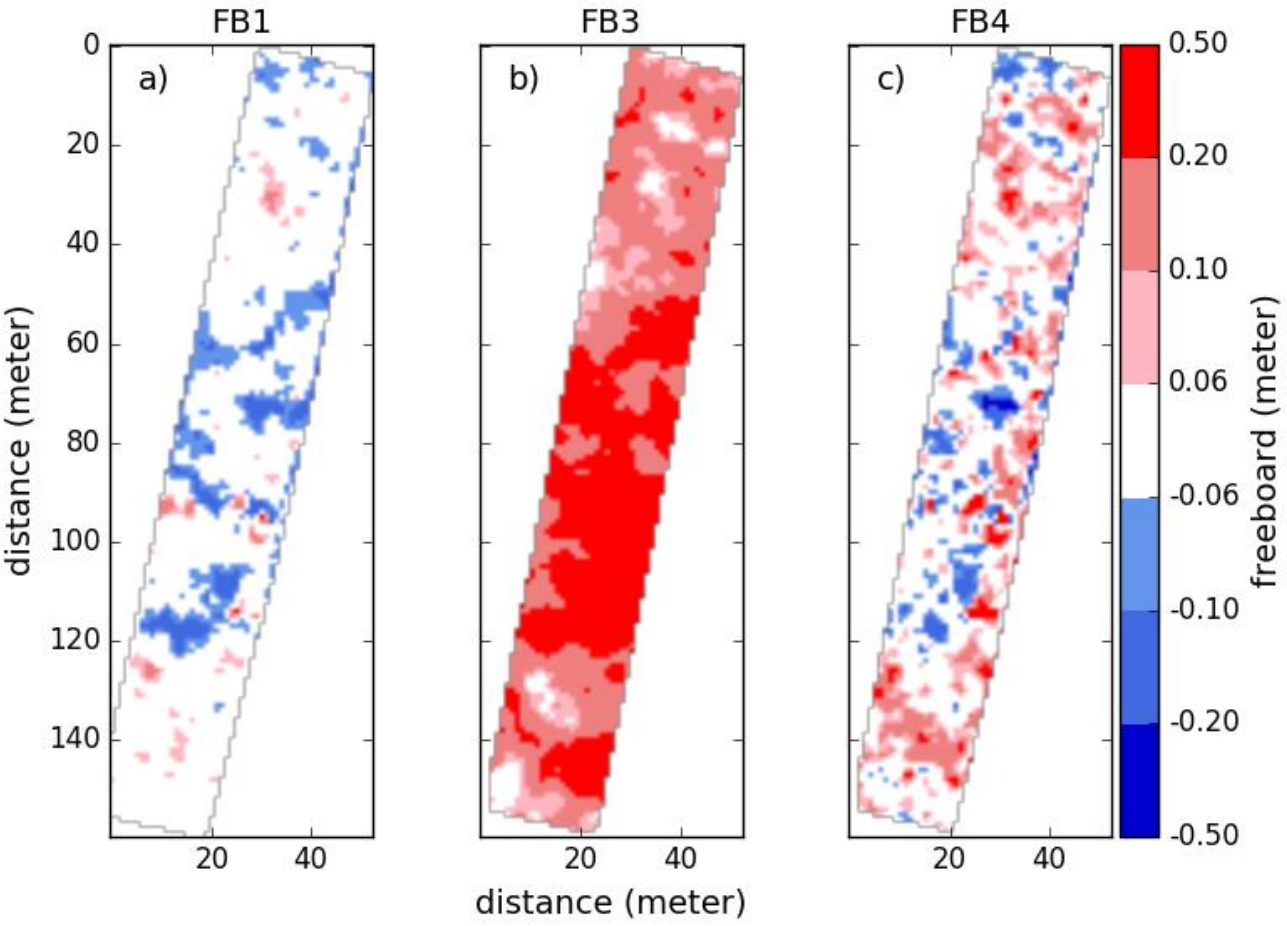


**Figure 7.** Freeboards (FB) over the 2-D survey field site. a) FB1 (calculated from SP snow depththickness, sea ice thickness from EM31 and densities of snow, ice and water), b) FB3 (surface elevation from ATM minus snow depththickness from SR), c) FB4 (surface elevation from ATM minus snow depththickness from SPR) of the 2-D survey field site. The white range represents the uncertainty of the freeboard estimation for FB1 ( $\pm 0.06\text{m}$ ) and is also applied for FB3 and FB4.

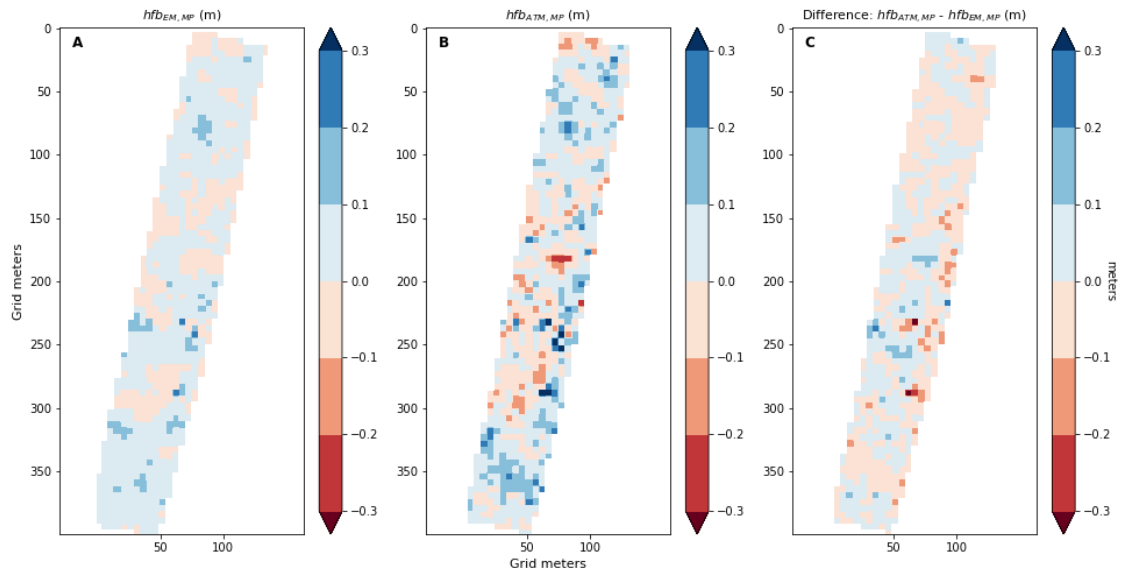
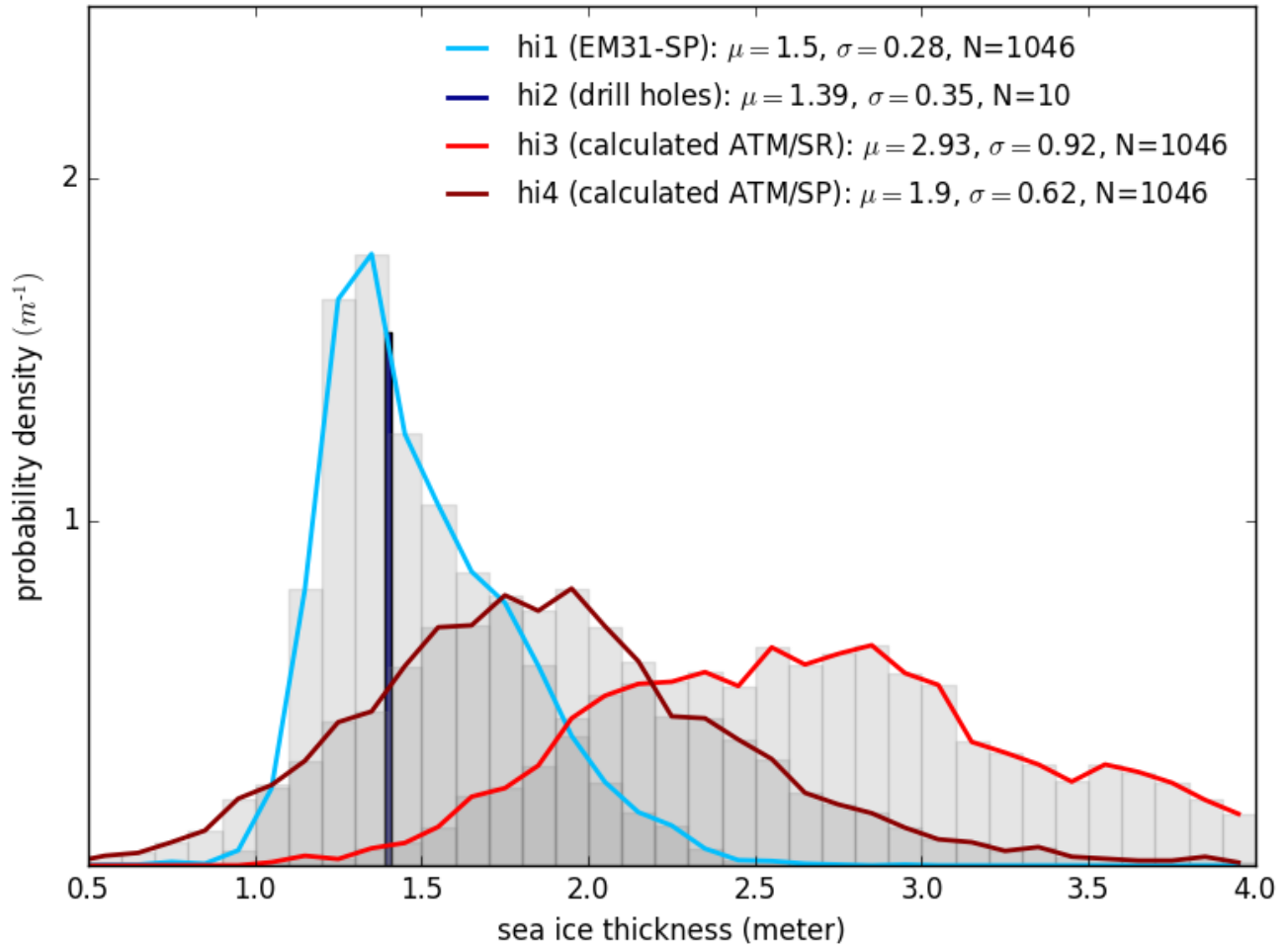
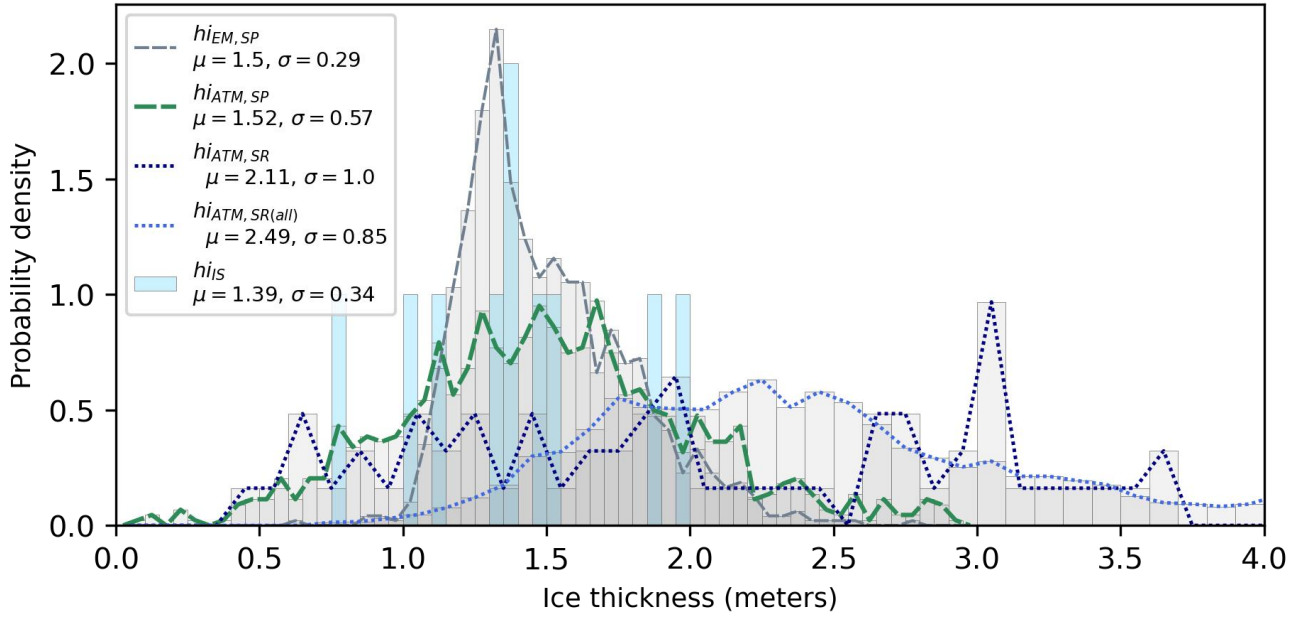


Figure 7: Ice freeboards ( $hfb$ ) over the survey site. a)  $hfb_{EM,SP}$  computed using Equation 3 with EM and snow probe data gridded at 5 m. b)  $hfb_{ATM,SP}$  using ATM surface elevation and MP snow depths gridded at 5 m. c) The difference between  $hfb_{EM,SP}$  and  $hfb_{ATM,SP}$ .



**Figure 8:** PDFs of sea ice thickness ( $h_i$ ) with given average values ( $\mu$ ), standard deviations ( $\sigma$ ), and number of measurements ( $N$ ) from the 2-D survey field site. *hi1* (light blue): Ice thickness calculated from EM31 total thickness and SP snow depth thickness; *hi2* (dark blue): Ice thickness from drill hole measurements; *hi3* (red): Ice thickness derived from ATM surface elevation and average snow depth thickness of SR measurements; *hi4* (dark red): Ice thickness derived from ATM surface elevation and snow depth thickness of SP measurements. Detailed descriptions of the methods are given in the text.



**Figure 8:** PDFs of sea ice thickness ( $h_i$ ) with given average values ( $\mu$ ), standard deviations ( $\sigma$ ), and number of measurements ( $N$ ) from the 2-D survey field site.  $h_{iEM,SP}$  (dashed gray): ice thickness calculated from EM31 total thickness and SP snow depth;  $h_{iATM,SR(all)}$  (dashed green): ice thick calculated from ATM surface elevation and SP snow depth in the 2D field;  $h_{iATM,SR}$  (dark blue dots): ice thickness calculated from ATM surface elevation and snow radar data using matched OIB ATM and radar observations in the 2D field;  $h_{iATM,SR(all)}$  (blue dots): ice thickness from all ATM surface elevation measurements in pass 2, and the mean of all radar snow depth estimates;  $h_{iS}$  (light blue bars): ice thickness measured in situ at drilling sites around the survey plot.

#### 4 Discussion and Conclusions

The mean and modal snow ~~depth~~<sup>thickness</sup> estimates derived from the snow radar were 0.125-0.16 m lower than the in-situ snow probe measurements, obtained at the 2-D survey field site. Over a larger regional scale of 10 km radius ~~from about~~ the *R/V Lance* location, snow ~~depth~~<sup>thickness</sup> estimates derived from the snow radar underestimate in situ snow probe-derived ~~thickness~~<sup>snow depth</sup> by 0.06 m, which is close to the measurement uncertainty of the snow radar system associated with its range resolution (Newman et al., 2014).



430 In radar altimetry, it is assumed that the radar signal penetrates completely through a dry snow pack and energy is reflected  
 431 from the snow/~~sea~~-ice interface, which represents the height of the sea ice-freeboard above local sea level. This assumption is  
 432 valid (Beaven et al., 1995) for a cold, dry and homogenous snow pack, typical of Arctic sea ice in winter. However, for snow  
 433 packs exhibiting high moisture content or higher densities (e.g. due to ice lenses/crusts), radar signals undergo absorption  
 434 within the snow volume (e.g., Kwok and Maksym, 2014; Ricker et al., 2015). Recent studies suggest reduced signal penetration  
 435 into the snow pack, with a more diffuse snow/~~sea~~-ice interface, on both Arctic and Antarctic sea ice (Gerland et al., 2013;  
 436 Kwok and Kacimi, 2018), especially if the snow pack is saline (Nandan et al., 2020; Nandan et al., 2017) or very deep with  
 437 ice lenses present (King et al., 2018). In addition, deep snow pushes the ice surface below the water level, leading to negative  
 438 freeboard and induces flooding and ~~formation of highly-saline slush layers-slushy, snow-ice formation~~ in the basal layers of  
 439 the snow pack, which, when measured with a radar altimeter system, can result in a dominant scattering horizon above the true  
 440 snow/ice interface (Nandan et al., 2020), and hence an overestimation of ice freeboard and thus sea ice thickness, and an  
 441 underestimate of ~~total~~ snow ~~depth~~thickness.  
 442 On FYI, overlying snow also wicks brine upwards from the sea ice surface during freeze-up, producing saline snow layers,  
 443 predominately observed in the bottom-most 0.06-0.08 m of the snow pack (Drinkwater and Crocker, 1988; Geldsetzer et al.,  
 444 2009; Nandan et al., 2016, 2017, 2020). ~~The salinity profile of-anthe ice core, taken on 5 March 2015 at-in the vicinity of the~~  
 445 ~~2-D survey field site, shows a typical C-shape profile with relatively high salinity values up to 11.3 psu at the top and 5.8 psu~~  
 446 ~~at the bottom, respectively, and lower values of between 1.3 psu and 4.3 psu in the middle sections of the ice core (see Figure~~  
 447 ~~910 in Appendix) suggesting that the 2-D survey field site on the ice floe comprised of FYI. Sea-ice salinity observations from~~  
 448 ~~the 1 m thick FYI floe, collected on 5 and 23 March 2015, show\_a salinityies of > 11 psu in the uppermost 0.10 m sea ice~~  
 449 ~~layers (Figure 10 in Appendix).~~ Snow salinity observations from snow covers (0.26 m and 0.34 m thick) overlying the FYI  
 450 floe indicate highly-saline, 0.10 m deep basal layers in both snow covers, by up to 10 psu. Additionally, one-third of the drill-  
 451 holes at the 2D field site indicated flooding of the snow pack, and negative freeboard, which induced the formation of highly  
 452 saline and saturated slush in the basal snow layers. ~~P~~The presence of ~~this slushy snow-ice layers~~s at the 2D field site resulted in  
 453 a challenging geophysical setting for the measurement of ~~total~~ snow and ice thickness using remote sensing techniques.  
 454 Previous studies (Barber et al., 1998; Barber and Nghiem, 1999; Nghiem et al., 1995; Geldsetzer et al., 2009; Nandan et al.,  
 455 2017; Nandan et al., 2020) have reported the impact of saline snow on FYI, which alters the geophysical, thermodynamic,  
 456 dielectric and radar scattering properties of the snow cover, thereby- impacting radar signal penetration through the snow pack.  
 457 Nandan et al. (2017) ~~and (2020)~~ showed that a saline snow cover on a ~~positive freeboard, landfast~~ FYI setting, induced by  
 458 upward ~~snow~~ brine wicking from the sea ice surface, shifted the main radar -scattering horizon away from the snow/~~sea~~-ice  
 459 interface by up to 0.07 m, ~~and weakened the signal arising from the saline scattering horizon~~. In these studies, covering the  
 460 Canadian (Nandan et al., 2017) and the Atlantic (Nandan et al., 2020) sectors of the Arctic, the conditions at the survey field  
 461 site included saline, wet, and deep snow which impacted the accuracy of the snow ~~depth~~thickness derived from the snow radar  
 462 signal. In the Nandan et al. (2020) case study from the N-ICE2015 experiment, they demonstrated significant overestimations

in FYI thickness by up to 95% between simulated FYI thickness, snow radar and ATM-derived FYI thickness. They simulated the Ku-band radar scattering horizon from 0.36 m and 0.45 m deep snow on 0.69 m and 0.92 m ~~thick~~ ice, exhibiting negative freeboards by 0.04 m and 0.07 m, respectively. Measured snow salinities towards the basal layers overlying slush layers, were found to be high, up to 25 psu. They found that the FYI thickness overestimations was a result of vertical shift in the radar scattering horizon, caused by upward snow brine wicking from the ~~negative freeboard induced slushy snow layers,~~ caused by negative freeboards.

~~Our study~~ Observations from our study indicate the impact of saline snow conditions overlying slush layers ~~our study~~ shows that saline snow conditions can lead to the observed underestimation of snow radar-derived total snow depth. This is likely thickness by the radar, due to a combination of factors including reflection from a scattering horizon in the snow pack that is above the main snow/ice interface, a diffuse scattering horizon within the snow volume, and potential errors in the height of the snow/ice interface picked in individual snow radar echoes. Although, we do not have any direct measurements of slush salinity, nor any indication of whether the high basal snow salinity values observed from our survey site and also reported in Nandan et al. (2020) are due to basal snow brine wicking from the slush layers. Even though the snow radar underestimated mean snow ~~depth~~ thickness by between 0.06 m and 0.126 m across the 2-D survey field site and the regional survey, the radar was able to fully reproduce the snow ~~depth~~ thickness variability, when compared to in situ measurements (standard deviations of 0.16 m and 0.15 m for the survey field, respectively; see Figure 3). Thus, we can report that the airborne snow radar is capable of measuring meaningful snow ~~depth~~ thickness distributions even in challenging snow pack conditions. However, ambiguous radar signal penetration through slushy layers (caused by sea ice flooding) and saline snow covers (caused by brine wicking from sea ice surface) may introduce a potential bias in accurate estimates of ~~total snow~~ depth ~~thickness~~. For a radar altimeter, the main scattering horizon within the snow volume is not just a function of snow ~~depth~~ thickness, but also depends on the thermodynamic properties of the snow cover (i.e., snow temperature, density, salinity, wetness, roughness, and grain microstructure). Further research is required to understand the relationship between the main scattering horizon and variability in snow cover properties.

Biases caused by uneven penetration of radar altimeter signals within slushy and saline layers in the snow pack will also have implications on estimates of snow and sea ice thickness measurements from currently operational satellite-based radar altimeters such as SARAL AltiKa (Ka-band), CryoSat-2 and Sentinel-3A/B (Ku-band), and the ESA's ~~forthup~~coming Ku- and Ka-band dual-frequency satellite radar altimeter mission CRISTAL. King et al. (2018) reported underestimation of sea ice thickness derived from CryoSat-2 data caused by negative freeboards in the same region as was investigated in our study. A detailed quantification of the contributions to the error budget associated with freeboard retrieval from CryoSat-2 was made by the ESA CryoVal-SI project team and is described in Ricker et al. (2014) and Haas et al. (2016). To examine the impact of a deep snow pack with saline and/or flooded ~~snow/ice-snow ice~~ interface, we show as an example the CryoSat-2 sea ice products provided by the NASA Goddard Space Flight Center (GSFC, Kurtz et al., 2014) for the region surrounding *R/V Lance* location in March 2015 (Figure 109). ~~It is striking that for this region~~ Noticeably, the CryoSat-2 sea ice freeboard and derived

sea ice thickness from this region demonstrate large spatial variability. Freeboard measurements are up to with measurements by is up to 0.3 m (Figure 109b), and the derived sea ice thickness is overestimated by over 1.0 m (Figure 910c), when compared with the in situ results reported in Rösel et al., 2018). Modelled The assumed snow depththicknesses of 0.15 m and 0.37 m (derived from Warren et al., 1999; Kurtz et al., 2014, Figure 109a) are underestimated when compared to the observed in situ snow depththickness, which averaged 0.55 m.

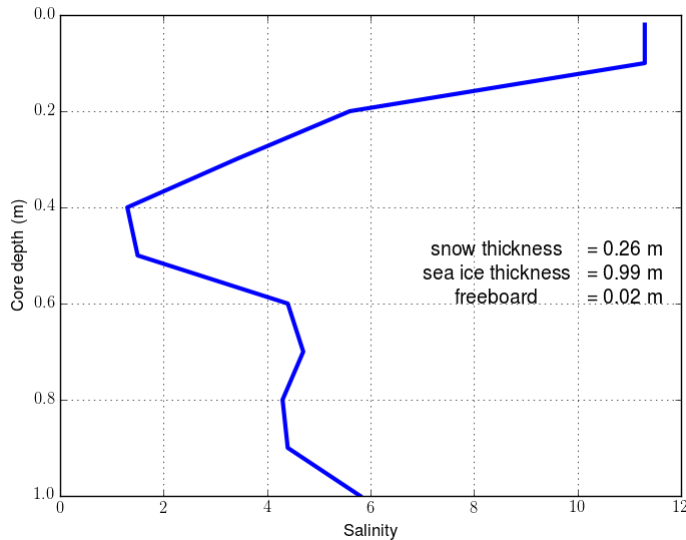


**Figure 9.** Salinity profile and auxiliary data of an ice core, taken on 5 March 2015 within the vicinity of the 2-D survey field.

-Sea ice parameters from the GSFC CryoSat-2 are derived with a waveform fitting procedure using an empirical waveform model (Sallila et al., 2019), which should account for snow geophysical properties. However, presently operational CryoSat-2 retracker algorithms or empirical models (e.g. Hendricks et al., 2010; Ricker et al., 2014; Kurtz et al., 2014) do not account for snow pack flooding as a source of error, affecting the accuracy of sea ice freeboard and thickness estimates. Moreover, since our survey site was also drifting, we acknowledge the impact of sea ice dynamics also affecting the correlations between in situ measurements and satellite-derived estimates, both acquired at different times (Tilling et al., 2018).-But, to our knowledge, currently, none of the conventional CryoSat 2 retracker algorithms (Hendricks et al. 2010; Ricker et al., 2014) or the empirical models (Kurtz et al., 2014) include flooding in the snow pack as a consideration. All of these-This issues could cause misinterpretation of both, airborne and satellite radar altimeter signals, especially in complicated areas where sea ice undergoes drift and frequent flooding of snow cover. We, therefore, recommend future improvements in sea ice freeboard and thickness retrieval algorithms. flooding of the snow cover has been observed such as in the Atlantic sector of the Arctic, and

also in parts of the Weddell and Bellingshausen Seas in the Southern Ocean which results in an overestimation of sea ice thickness. Our study suggests that this issue should to be considered and improved in the future.

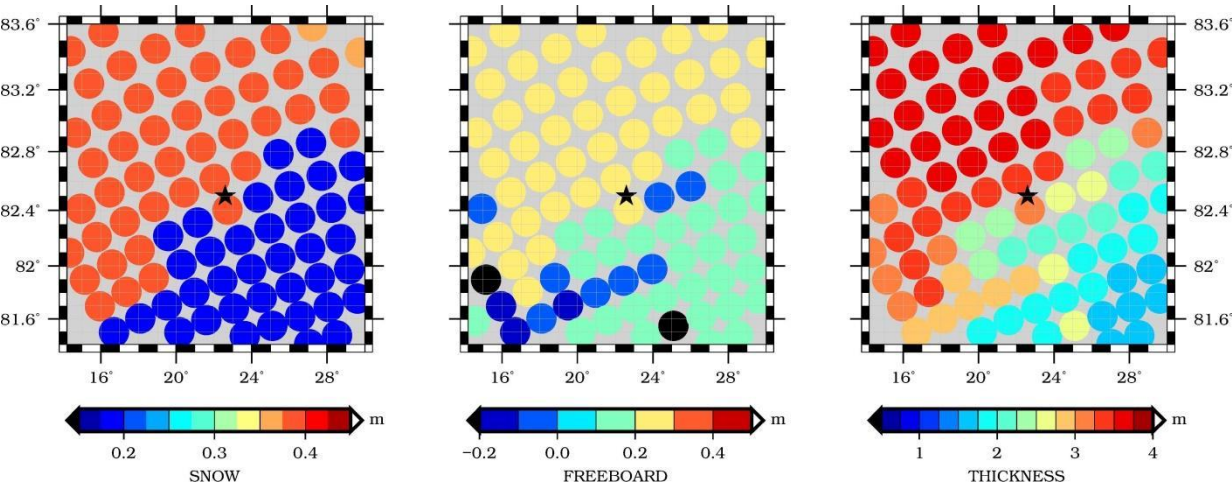


**Figure 109:** Results from CryoSat-2 sea ice products from GSFC, averaged for the month March 2015 for a region of 250 km × 250 km over the in-situ site in the Norwegian Arctic for a) snow ~~depth~~thickness, b) sea ice freeboard, c) sea ice thickness. The position of *R/V Lance* is marked with a star.

**Acknowledgements:** The authors would like to thank the two revisers for their valuable comments which helped is to improve the original manuscript. We thank all crew members of *R/V Lance* and all scientific staff involved in N-ICE2015 for their support and help during the fieldwork. This work was supported by the Norwegian Polar Institute’s Center for Ice, Climate and Ecosystems (ICE) through the project N-ICE2015 and the project ID Arctic (Norwegian Ministries of Foreign Affairs and Climate and Environment; SG, AR). VN acknowledges Post-Doctoral Fellowship grant to Canada’s Marine Environmental Observation, Prediction and Response Network (MEOPAR). SLF was supported under NOAA grant NA14NES4320003, and the NOAA Product Development, Readiness, and Application (PDRA)/Ocean Remote Sensing (ORS) program. GS acknowledges support by the Trans regional Collaborative Research Center (TR 172) “Arctic Amplification: Climate Relevant Atmospheric and SurfaCe Processes, and Feedback Mechanisms (AC)3”, funded by the German Research Foundation DFG. The contribution of AS to this study was funded by the Research Council of Norway through the Nansen Legacy project (NFR-276730). N-ICE2015 acknowledges the in-kind contributions provided by other national and international projects and participating institutions, through personnel, equipment and other support. N-ICE2015 data is available through <http://data.npolar.no/> and NASA’s OIB data is publicly available via <https://nsidc.org/icebridge/portal/map>.

## References

- Barber, D., Fung, A., Grenfell, T., Nghiem, S., Onstott, R., Lytle, V., Perovich, D., and Gow, A.: The Role of Snow on Microwave Emission and Scattering over First-Year Sea Ice, *IEEE Transactions on Geoscience and Remote Sensing*, 36, 1750–1763, 1998.
- Barber, D. G. and Nghiem, S. V.: The role of snow on the thermal dependence of microwave backscatter over sea ice, *Journal of Geophysical Research: Oceans*, 104, 25 789–25 803, 1999.
- Beaven, S. G., Lockhart, G. L., Gogineni, S. P., Hossetnmostafa, A. R., Jezek, K., Gow, A. J., Perovich, D. K., Fung, A. K., and Tjuatja, S.: Laboratory measurements of radar backscatter from bare and snow-covered saline ice sheets, *International Journal of Remote Sensing*, 16, 851–876, 1995.
- Dominguez, R.: Icebridge DMS L1B geolocated and orthorectified images, (IODMS1B), Boulder, Colorado USA. NASA National Snow and Ice Data Center Distributed Active Archive Center., 2010, updated 2018.
- Drinkwater, M. R. and Crocker, G.: Modelling Changes in Scattering Properties of the Dielectric and Young Snow-Covered Sea Ice at GHz Frequencies, *Journal of Glaciology*, 34, 274–282, 1988.
- Eicken, H., Grenfell, T. C., Perovich, D. K., Richter-Menge, J. A., and Frey, K.: Hydraulic controls of summer Arctic pack ice albedo, *Journal of Geophysical Research: Oceans*, 109, 2004.
- Farrell, S. L., Kurtz, N., Connor, L. N., Elder, B. C., Leuschen, C., Markus, T., McAdoo, D. C., Panzer, B., Richter-Menge, J., and Sonntag, J. G.: A First Assessment of IceBridge Snow and Ice Thickness Data Over Arctic Sea Ice, *IEEE Transactions on Geoscience and Remote Sensing*, 50, 2098–2111, 2012.
- Geiger, C., Müller, H.-R., Samluk, J. P., Bernstein, E. R., and Richter-Menge, J.: Impact of spatial aliasing on sea-ice thickness measurements, *Annals of Glaciology*, 56, 53–362, 2015.
- Geldsetzer, T., Langlois, A., and Yackel, J.: Dielectric properties of brine-wetted snow on first-year sea ice, *Cold Regions Science and Technology*, 58, 47–56, 2009.
- Gerland, S., Renner, A. H. H., Spreen, G., Wang, C., Beckers, J., Dumont, M., Granskog, M. A., Haapala, J., Haas, C., Helm, V., Hudson, S. R., Lensu, M., Ricker, R., Sandven, S., Skourup, H., and Zygmuntowska, M.: In-situ calibration and validation of CryoSat-2 Observations Over Arctic sea ice north of Svalbard, in: *Proc. Earth Observation and Cryosphere Science Conf.*, Frascati, Italy, 13-16 November 2012, ESA SP-712, 2013.
- Gerland, S., Granskog, M. A., King, J., and Rösel, A.: [data set] N-ICE2015 ice core physics: temperature, salinity and density, <https://doi.org/10.21334/npolar.2017.c3db82e3>, 2017.
- Giles, K.A., Laxon, S.W., Wingham, D.J., Wallis, D.W., Krabill, W.B., Leuschen, C.J., McAdoo, D., Manizade, S.S. and Raney, R.K., 2007. Combined airborne laser and radar altimeter measurements over the Fram Strait in May 2002. *Remote Sensing of Environment*, 111(2-3), pp.182-194.
- Graham, R. M., Cohen, L., Petty, A. A., Boisvert, L. N., Rinke, A., Hudson, S. R., Nicolaus, M., and Granskog, M. A.: Increasing frequency and duration of Arctic winter warming events, *Geophysical Research Letters*, 44, 6974–6983, 2017.

583 Granskog, M., Assmy, P., Gerland, S., Spreen, G., Steen, H., and Smedsrud, L.: Arctic Research on Thin Ice: Consequences  
584 of Arctic Sea Ice Loss, *Eos, Transactions American Geophysical Union*, 97, 2016.

585 Granskog, M. A., Rösel, A., Dodd, P. A., Divine, D., Gerland, S., Martma, T., and Leng, M. J.: Snow contribution to first-year  
586 and second-year Arctic sea ice mass balance north of Svalbard, *Journal of Geophysical Research: Oceans*, 122, 2539–2549,  
587 2017.

588 Grenfell, T. C. and Maykut, G. A.: The Optical Properties of Ice and Snow in the Arctic Basin, *Journal of Glaciology*, 18,  
589 445–463, 1977.

590 Haas, C., Gerland, S., Eicken, H., and Miller, H.: Comparison of sea-ice thickness measurements under summer and winter  
591 conditions in the Arctic using a small electromagnetic induction device, *GEOPHYSICS*, 62, 749–757, 1997.

592 Haas, C., Lobach, J., Hendricks, S., Rabenstein, L., and Pfaffling, A.: Helicopter-borne measurements of sea ice thickness,  
593 using a small and lightweight, digital EM system, *Journal of Applied Geophysics*, 67, 234–241, 2009.

594 Haas, C., Hendricks, S., Ricker, R., King, J., Beckers, J. and Skourup, H., and et al.: CryoVal-SI: CryoSat Sea Ice Product  
595 Validation using CryoVex and IceBridge campaign data, Techreport, Norwegian Polar Institute, 2016.

596 Hendricks, S., Stenseng, L., Helm, V., and Haas, C.: Effects of Surface Roughness on Sea Ice Freeboard Retrieval with an  
597 Airborne Ku-Band SAR Radar Altimeter, in: *Geoscience and Remote Sensing (IGARSS 2010)*, IEEE International  
598 Symposium., 2010.

599 Holt, B., Johnson, M. P., Perkovic-Martin, D., and Panzer, B.: Snow depth on Arctic sea ice derived from radar: In situ  
600 comparisons and time series analysis, *Journal of Geophysical Research: Oceans*, 120, 4260–4287, 2015.

601 Kern, S., Khvorostovsky, K., Skourup, H., Rinne, E., Parsakhoo, Z. S., Djepa, V., Wadhams, P., and Sandven, S.: The impact  
602 of snow depth, snow density and ice density on sea ice thickness retrieval from satellite radar altimetry: results from the ESA-  
603 CCI Sea Ice ECV Project Round Robin Exercise, *The Cryosphere*, 9, 37–52, 2015.

604

605 King, J., Howell, S., Derksen, C., Rutter, N., Toose, P., Beckers, J. F., Haas, C., Kurtz, N., and Richter-Menge, J.:  
606 Evaluation of Operation IceBridge quick-look snow depth estimates on sea ice, *Geophysical Research Letters*, 42, 9302–9310,  
607 2015.

608 King, J., Skourup, H., Hvidegaard, S. M., Rösel, A., Gerland, S., Spreen, G., Polashenski, C., Helm, V., and Liston, G. E.:  
609 Comparison of Free- board Retrieval and Ice Thickness Calculation From ALS, ASIRAS, and CryoSat-2 in the Norwegian  
610 Arctic to Field Measurements Made During the N-ICE2015 Expedition, *Journal of Geophysical Research: Oceans*, 123, 1123–  
611 1141, 2018.

612 Koenig, L., Martin, S., Studinger, M., and Sonntag, J.: Polar Airborne Observations Fill Gap in Satellite Data, *Eos*,  
613 *Transactions American Geophysical Union*, 91, 333–334, 2010.



614 Krabill, W., Abdalati, W., Frederick, E., Manizade, S., Martin, C., Sonntag, J., Swift, R., Thomas, R., and Yungel, J.: Aircraft  
 615 laser altimetry measurement of elevation changes of the greenland ice sheet: technique and accuracy assessment, *Journal of*  
 616 *Geodynamics*, 34, 357–376, 2002.

617 Kurtz, N. T., Farrell, S. L., Studinger, M., Galin, N., Harbeck, J. P., Lindsay, R., Onana, V. D., Panzer, B., and Sonntag, J. G.:  
 618 Sea ice thickness, freeboard, and snow depth products from Operation IceBridge airborne data, *The Cryosphere*, 7, 1035–  
 619 1056, 2013.

620 Kurtz, N. T., Galin, N., and Studinger, M.: An improved CryoSat-2 sea ice freeboard retrieval algorithm through the use of  
 621 waveform fitting, *The Cryosphere*, 8, 1217–1237, <https://doi.org/10.5194/tc-8-1217-2014>, 2014.

622 Kwok, R.: Simulated effects of a snow layer on retrieval of CryoSat-2 sea ice freeboard, *Geophysical Research Letters*, 41,  
 623 5014–5020, 2014.

624 Kwok, R. and Kacimi, S.: Three years of sea ice freeboard, snow depth, and ice thickness of the Weddell Sea from Operation  
 625 IceBridge and CryoSat-2, *The Cryosphere*, 12, 2789–2801, 2018.

626 Kwok, R. and Maksym, T.: Snow depth of the Weddell and Bellingshausen sea ice covers from IceBridge surveys in 2010 and  
 627 2011: An examination, *Journal of Geophysical Research: Oceans*, 119, 4141–4167, 2014.

628 Kwok, R., Kurtz, N. T., Brucker, L., Ivanoff, A., Newman, T., Farrell, S. L., King, J., Howell, S., Webster, M. A., Paden, J.,  
 629 Leuschen, C., Macgregor, J. A., Richter-Menge, J., Harbeck, J., and Tschudi, M.: Inter-comparison of snow depth retrievals  
 630 over Arctic sea ice from radar data acquired by Operation IceBridge, *The Cryosphere*, 11, 2571–2593, 2017.

631 Lawrence, I.R., Tsamados, M.C., Stroeve, J.C., 2, Armitage, T.W.K., and Ridout, A.L.: Estimating snow depth over Arctic sea  
 632 ice from calibrated dual-frequency radar freeboards. *The Cryosphere*, 12, 3551–3564, 2018.

633 Marshall, H. P., Koh, G., Sturm, M., Johnson, J., Demuth, M., Landry, C., Deems, J., and Gleason, A.: Spatial variability of  
 634 the snowpack: Experiences with measurements at a wide range of length scales with several different high precision  
 635 instruments, *Proc. ISSW 2006*, pp. 359–364, 2006.

636 Massom, R. A., Eicken, H., Hass, C., Jeffries, M. O., Drinkwater, M. R., Sturm, M., Worby, A. P., Wu, X., Lytle,  
 637 V. I., Ushio, S., Morris, K., Reid, P. A., Warren, S. G., and Allison, I.: Snow on Antarctic sea ice, *Reviews of Geophysics*,  
 638 39, 413–445, 2001.

639 Merkouriadi, I., Cheng, B., Graham, R. M., Rösel, A., and Granskog, M. A.: Critical Role of Snow on Sea Ice Growth in the  
 640 Atlantic Sector of the Arctic Ocean, *Geophysical Research Letters*, 44, 10,479–10,485, 2017a.

641 Merkouriadi, I., Gallet, J.-C., Liston, G., Polashenski, C., Itkin, P., King, J., Espeseth, M., Gierisch, A., Oikkonen, A., Orsi,  
 642 A., and Gerland, S.: [data set] N-ICE2015 snow pit data, <https://doi.org/10.21334/npolar.2017.d2be5f05>, 2017b.

643 Merkouriadi, I., Gallet, J.-C., Liston, G. E., Polashenski, C., Rösel, A., and Gerland, S.: Winter snow conditions over the Arctic  
 644 Ocean north of Svalbard during the Norwegian young sea ICE (N-ICE2015) expedition, *Journal of Geophysical Research:*  
 645 *Atmospheres*, 122, 2017c.

646 Meyer, A., Sundfjord, A., Fer, I., Provost, C., Robineau, N. V., Koenig, Z., Onarheim, I. H., Smedsrud, L. H., Duarte, P.,  
647 Dodd, P. A., Graham, R. M., and Kauko, H.: Winter to summer hydrographic and current observations in the Arctic Ocean  
648 north of Svalbard, *Journal of Geophysical Research: Oceans*, 122, 2017.

649 Mundy, C. J., Ehn, J. K., Barber, D. G. and Michel, C.: 2007 Influence of snow cover and algae on the spectral dependence of  
650 transmitted irradiance through Arctic landfast first-year sea ice, *Journal of Geophysical Research: Oceans*, *J. Geophys. Res.: Oceans*, 112, C03007, 2007.

651

652

653 Nandan, V., Scharien, R. K., Geldsetzer, T., Kwok, R., Yackel, J. J., Mahmud, M., Rösel, A., Tonboe, R., Granskog, M.,  
654 Willatt, R., Stroeve, J., Nomura, D and Frey, M. "Snow Property Controls on Modeled Ku-Band Altimeter Estimates of First-  
655 Year Sea Ice Thickness: Case Studies from the Canadian and Norwegian Arctic," in *IEEE Journal of Selected Topics in*  
656 *Applied Earth Observations and Remote Sensing*, 13, 1082-1096, 2020.

657 Nandan, V., Geldsetzer, T., Islam, T., Yackel, J. J., Gill, J. P., Fuller, M. C., Gunn, G., and Duguay, C.: Ku-, X- and C-band  
658 measured and modeled microwave backscatter from a highly saline snow cover on first-year sea ice, *Remote Sensing of*  
659 *Environment*, 187, 62 – 75, 2016.

660 Nandan, V., Geldsetzer, T., Yackel, J., Mahmud, M., Scharien, R., Howell, S., King, J., Ricker, R., and Else, B.: Effect of  
661 Snow Salinity on CryoSat-2 Arctic First-Year Sea Ice Freeboard Measurements, *Geophysical Research Letters*, 2017.

662 Newman, T., Farrell, S. L., Richter-Menge, J., Connor, L. N., Kurtz, N. T., Elder, B. C., and McAdoo, D.: Assessment of  
663 radar-derived snow depth over Arctic sea ice, *Journal of Geophysical Research: Oceans*, 119, 8578–8602, 2014.

664 Nghiem, S. V., Kwok, R., Yueh, S. H., and Drinkwater, M. R.: Polarimetric signatures of sea ice: 2. Experimental observations,  
665 *Journal of Geophysical Research: Oceans*, 100, 13 681–13 698, 1995.

666 Ozsoy-Cicek, B., Ackley, S., Xie, H., Yi, D., and Zwally, J.: Sea ice thickness retrieval algorithms based on in situ surface  
667 elevation and thickness values for application to altimetry, *Journal of Geophysical Research: Oceans*, 118, 3807– 3822, 2013.

668 Perovich, D. K.: The Optical Properties of Sea Ice, vol. 96, CRREL ~~Megography~~ *Monography*, 1996. 31 pages.

669 Perovich, D. K.: Thin and thinner: Sea ice mass balance measurements during SHEBA, *Journal of Geophysical Research:*  
670 *Oceans*, 108, 2003.

671 Renner, A. H. H., Gerland, S., Haas, C., Spreen, G., Beckers, J. F., Hansen, E., Nicolaus, M., and Goodwin, H.: Evidence of  
672 Arctic sea ice thinning from direct observations, *Geophysical Research Letters*, 41, 5029–5036, 2014.

673 Ricker, R., Hendricks, S., Helm, V., Skourup, H., and Davidson, M.: Sensitivity of CryoSat-2 Arctic sea-ice freeboard and  
674 thickness on radar-waveform interpretation, *The Cryosphere*, 8, 1607–1622, 2014.

675 Ricker, R., Hendricks, S., Perovich, D. K., Helm, V., and Gerdes, R.: Impact of snow accumulation on CryoSat-2 range  
676 retrievals over Arctic sea ice: An observational approach with buoy data, *Geophysical Research Letters*, 42, 4447–4455, 2015.

677 Rinke, A., Maturilli, M., Graham, R. M., H., M., Handorf, D., Cohen, L., Hudson, S. R., and Moore, J. C.: Extreme cyclone  
678 events in the Arctic: Wintertime variability and trends, *Environmental Research Letters*, 12, 2017.

679 Rösel, A., King, J., Doulgeris, A. P., Wagner, P. M., Johansson, A. M., and Gerland, S.: Can we extend local sea-ice  
680 measurements to satellite scale? An example from the N-ICE2015 expedition, *Annals of Glaciology*, pp. 1–10, 2017.

681 Rösel, A., Itkin, P., King, J., Divine, D., Wang, C., Granskog, M. A., Krumpen, T., and Gerland, S.: Thin sea ice, thick snow  
682 and widespread negative freeboard observed during N-ICE2015 north of Svalbard, *Journal of Geophysical Research: Oceans*,  
683 123, 2018.

684 Sallila, H., Farrell, S.L., McCurry, J. and Rinne, E., 2019. Assessment of contemporary satellite sea ice thickness products for  
685 Arctic sea ice. *The Cryosphere*, 13(4), pp.1187-1213.

686 Skourup, H., Farrell, S.L., Hendricks, S., Ricker, R., Armitage, T.W., Ridout, A., Andersen, O.B., Haas, C. and Baker, S.,  
687 2017. An Assessment of State-of-the-Art Mean Sea Surface and Geoid Models of the Arctic Ocean: Implications for Sea Ice  
688 Freeboard Retrieval. *Journal of Geophysical Research: Oceans*, 122(11), pp.8593-8613.

689 Sturm, M.: Winter snow cover on the sea ice of the Arctic Ocean at the Surface Heat Budget of the Arctic Ocean (SHEBA):  
690 Temporal evolution and spatial variability, *Journal of Geophysical Research: Oceans*, 107, 2002.

691 Sturm, M. and Holmgren, J.: Self-recording snow depth probe, Tech. rep., US patent number: 5,864,059., 1999.

692 Sturm, M., and Holmgren, J.: An automatic snow depth probe for field validation campaigns. *Water Resources Research*, 54,  
693 9695–9701, 2018.

694 Wang, C., Cheng, B., Wang, K., Gerland, S., and Pavlova, O.: Modelling snow ice and superimposed ice on landfast sea ice  
695 in Kongsfjorden, Svalbard, *Polar Research*, 34, 2015.

696 Warren, S. G., Rigor, I. G., Untersteiner, N., Radionov, V. F., Bryazgin, N. N., Aleksandrov, Y. I., and Colony, R.: Snow  
697 Depth on Arctic Sea Ice, *Journal of Climate*, 12, 1814–1829, 1999.

698 Webster, M. A., Rigor, I. G., Nghiem, S. V., Kurtz, N. T., Farrell, S. L., Perovich, D. K., and Sturm, M.: Interdecadal changes  
699 in snow depth on Arctic sea ice, *Journal of Geophysical Research: Oceans*, 119, 5395–5406, 2014.

700 Woods, C. and Caballero, R.: The Role of Moist Intrusions in Winter Arctic Warming and Sea Ice Decline, *Journal of Climate*,  
701 29, 4473–4485, <https://doi.org/10.1175/jcli-d-15-0773.1>, 2016.

702 Willatt, R. C., Giles, K. A., Laxon, S. W., Stone-Drake, L., and Worby, A. P. (2009): Field investigations of Ku-band radar  
703 penetration into snow cover on Antarctic sea ice. *IEEE Transactions on Geoscience and remote sensing*, 48(1), 365-372. 2009.

704

705 Yan, J., Alvestegui, D. G.-G., McDaniel, J. W., Li, Y., Gogineni, S., Rodriguez-Morales, F., Brozena, J., and Leuschen, C. J.:  
706 Ultrawideband FMCW Radar for Airborne Measurements of Snow Over Sea Ice and Land, *IEEE Transactions on Geoscience*  
707 *and Remote Sensing*, 55, 834–843, 2017.

708 Zwally, H. J., Yi, D., Kwok, R., and Zhao, Y.: ICESat measurements of sea ice freeboard and estimates of sea ice thickness in  
709 the Weddell Sea, *Journal of Geophysical Research: Oceans*, 113, C02S15, 2008.

710

711 ~~Willatt, R. C., Giles, K. A., Laxon, S. W., Stone-Drake, L., & Worby, A. P. (2009). Field investigations of Ku-band~~  
712 ~~radar penetration into snow cover on Antarctic sea ice. *IEEE Transactions on Geoscience and remote sensing*,~~  
713 ~~48(1), 365-372.~~

714  
715 ~~Mundy C J, Ehn J K, Barber D C and Michel C 2007 Influence of snow cover and algae on the spectral dependence~~  
716 ~~of transmitted irradiance through Arctic landfast first-year sea ice *J. Geophys. Res.: Oceans* 112 C03007~~

717

718

719

720

721

722

723

724 **Appendix**

Drill-hole label	Ice thickness	<del>depth</del> Snow thickness	Freeboard	Flooded
D0	1.76	0.34	0.13	no
D1	1.48	0.49	0.01	no
D2	0.78	0.30	0.02	no
D3	1.03	0.57	-0.03	no
D4	1.34	0.38	0.03	no
D5	1.65	0.83	-0.11	yes
D6	1.35	0.76	-0.09	yes
D7	1.36	0.28	0.07	no
D8	1.15	0.51	-0.03	yes
D9	1.96	0.51	0.07	no
Mean (Stddev)	1.39 (0.35)	0.50 (0.19)	0.01 (0.07)	

725

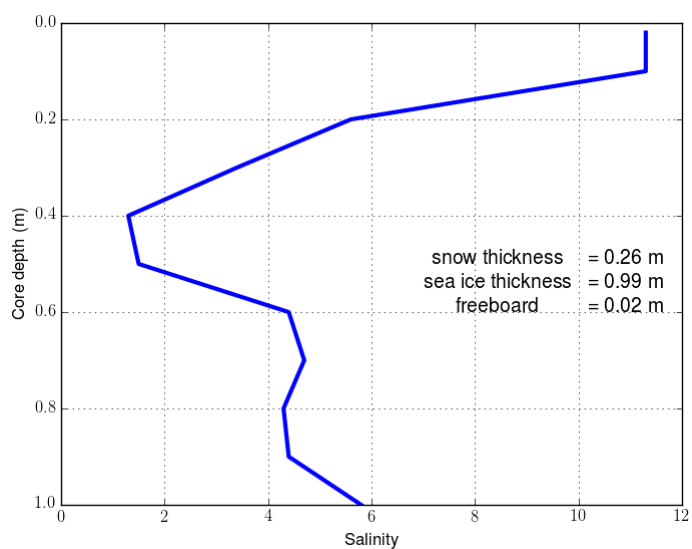
726 **Table 23.** Measurements acquired at 10 drill-hole sites located randomly across the 2-D survey field site. All values are given  
727 in meters.

728

729

730

Figure 10. Salinity profile and auxiliary data of an ice core, taken on 5 March 2015 within the vicinity of the 2-D survey field.



758  
759  
760  
761